

Research article

Early Paleozoic mafic intraplate magmatism in the Binaloud zone, NE Iran: Implications for the long-lived mantle plume activity in the northern margin of Gondwana

Fatemeh Sepidbar^a, Seyed Masoud Homam^{a,*}, Guanghui Wu^b, Robert Moritz^c,
Hamid Hafezimoghadas^a

^a Department of Geology, Faculty of Science, Ferdowsi University of Mashhad, Iran

^b School of Geoscience and Technology, Southwest Petroleum University, Chengdu 610500, China

^c Department of Earth Sciences, University of Geneva, Geneva, Switzerland



ARTICLE INFO

Keywords:

Continental rifting
Mantle plume
Silurian
Binaloud

ABSTRACT

Documentation of continental rifting processes such as mantle plume activity is important for understanding the nature and evolution of tectonic plates. In this study, we report detailed petrological, geochronological, geochemical, Sr–Nd isotope, and mineral chemical data for basalt, and coarse- and fine-grained gabbro from the Binaloud zone of the Alborz, which is the easternmost extension of the Avalonian-Cadomian Orogenic Belts and the western parts of Indo-Australia Orogenic Belt, central-east Asia. Uranium–lead zircon dating of fine- and coarse-grained gabbro indicates that they have been formed at 461.8 ± 8.2 and 435.0 ± 4.5 Ma, respectively. The basalt and gabbro have large variations in elemental and isotopic compositions, with 44.0–50.0 wt% SiO₂, 124–411 ppm Sr, and $\epsilon\text{Nd}(t)$ of +0.1 to +3.3. All the rocks show OIB-like or transitional OIB–/E-MORB-like geochemical characteristics, without noticeable Nb–Ti depletion, diagnostic of an intraplate affinity. Whole-rock geochemical and isotopic compositions combined with mineral compositions suggest that both basalt and gabbro have been generated by a plume/asthenospheric mantle (OIB-type) source mixed with enriched sub-continental lithospheric mantle components. Partial melting of such a source in the transitional spinel-garnet stability field was followed by different degrees of fractional crystallization of olivine, clinopyroxene, and plagioclase. Our study demonstrates that roll-back of the subducting Tornquist (Eastern Ipeous ocean) oceanic lithosphere has been followed by plume activity, continental rifting and Paleo-Tethys opening during the Silurian period.

1. Introduction

An important query in the Earth's sciences is how continental breakup is caused (e.g., [Condie, 2016](#)). Globally, rifted basins are characterized by up to 15 km of under-plated mafic crust and submarine seaward-dipping indicators, which are thick wedges of mainly volcanic material that thickens oceanward within the continent-ocean transition ([Planke et al., 2000](#)). It is assumed that the basalts are generally tholeiitic or/alkaline in composition and were formed during the initial stages of mantle plume activity, when it impinged the oceanic crust ([Richards et al., 1989](#)). Otherwise, it has also been suggested that subduction of a spreading center or other changes in plate boundary dynamics can lead to continental breakup (e.g. [Bradshaw, 1989](#)). A

favorable tectonic setting for the petrogenesis of alkaline basalts is roll-back of a subducting slab, leading to back-arc extension, followed by plume mantle activity, rifting and continental breakup ([Moghadam et al., 2018](#)).

A number of Proto-Tethys suture zones and associated orogenic belts have been identified and dated as Neoproterozoic, Cambrian, Ordovician and Silurian. They are known as Iapetus and are associated with the Cadomian-Avalonian orogenic belt in the west and the Kunlun-Qilian-Qinling belt belonging to the North Indo-Australia orogeny, central-east Asia, in the east ([Fig. 1](#)). The Cadomian-Avalonian belt extends from Newfoundland to northern Nova Scotia, southern New Brunswick, Massachusetts, Oaxaca, Iberia, France, the Alps, SE Europe, Turkey and to Iran. The Kunlun-Qilian-Qinling belt extends from North China,

* Corresponding author.

E-mail address: homam@um.ac.ir (S.M. Homam).

possibly South China, through Tarim, Qaidam, Indochina, North Qiangtang, and Karakum to Iran in the northern margin of Gondwana. Other authors have called it the Asian-Hun Superterrane (Metcalfe, 2021).

The Avalonian-Cadomian Orogen formed to the south of the Iapetus Ocean along the Gondwana margin. It consists of an older Proterozoic basement on which a convergent continental margin with a magmatic arc was developed (Fig. 1; Cawood et al., 2021). These major paleogeographic blocks are well known, but the geodynamic causes, kinematics, and precise timing of the transition from the Cadomian accretionary convergent-margin processes to rifting development remain open to question. On the one hand, the onset of rifting near the end of the Cadomian orogeny was caused by an upwelling mantle plume that affected the Gondwana margin at around 540 Ma (e.g., Floyd et al., 2000; Winchester et al., 2006). On the other hand, a second model proposes that retreat of an oceanic plate, which was subducting beneath northern Gondwana until the early Ordovician, has been responsible for rifting (Arenas et al., 2007; Díez Fernández et al., 2012; Nance et al., 2012). In both interpretations, the results were extension, continental thinning and rifting and juvenile crustal addition (Miskovic and Schaltegger, 2009).

Iran represents the easternmost expression of the Avalonian-Cadomian Orogenic belt (Moghadam et al., 2016, 2017, Honarmand et al., 2018; Sepidbar et al., 2020). It is characterized by arc-related igneous and sedimentary successions that range in age from ca. 630 to 500 Ma, but with most intense magmatism between 570 and 530 Ma (Ramezani and Tucker, 2003; Honarmand et al., 2018). Lithospheric extension is recorded by rift-related bimodal magmatism and sedimentation during ca. 530–490 Ma, (e.g., Sepidbar et al., 2020), followed by rift-related alkaline magmatism and sedimentation from Ordovician (Derakhshi et al., 2022) to Carboniferous (Saccani et al., 2013; Stöcklin, 1968). However, it is still unknown whether the opening of the Paleo-Tethys Ocean was controlled by mantle-plume, or by subduction-related back-arc extension.

The Binaloud zone of northeast Iran has been considered to be a part of the northern margin of Gondwana, based on a robust agreement of the palaeomagnetic poles of Iran and Gondwana for the Late Ordovician-earliest Carboniferous (Muttoni et al., 2009). Previous studies have reported paleontological, sedimentological (Jamshidipour, 2022), and geochemical data. The few reported $^{40}\text{Ar}/^{39}\text{Ar}$ ages of hornblende from the volcanic rocks in the Binaloud zone indicate a Middle Permian age for the olivine cumulate rocks (Topuz et al., 2018). By contrast, there are only rare data for the Silurian magmatism. To fill this gap and to place new constraints on the composition, age and geodynamic setting of magmatism during the Early Paleozoic, we report in this study new whole-rock major and trace element compositions, Sr–Nd isotope data, and zircon U–Pb ages for a variety of rock types from the Paleozoic units of the Binaloud zone. The timing and tectonic environment of the mantle plume activity, as well as the understanding of the corresponding tectonic implications about the breakup of Gondwana and the opening of the Paleo-Tethys Ocean are major issues, and remain unclear. In this paper, we demonstrate that although the Tornquist slab roll-back and back-arc opening took place in the eastern part of the Cadomian-Avalonian orogenic belt during the Late Neoproterozoic-Early Cambrian, both the Binaloud gabbro and basalt are products of mantle plume activity in a continental setting during the Silurian.

2. Geological background

The oldest rock strata in Iran consist of Late Neoproterozoic–Cambrian sandstone with minor carbonate and volcanic rocks, which are unconformably overlying a granitic basement. On the basis of fossils and regional correlations, this ~1 km thick basal sequence, which includes the Kahar, Bayandor, Soltanieh, Barut, and Lalun formations, is overlain conformably by an incomplete up to 3 km thick Paleozoic succession consisting of carbonate and clastic rocks (Figs. 3 and 4; Stöcklin, 1968). Scattered Paleozoic rock successions

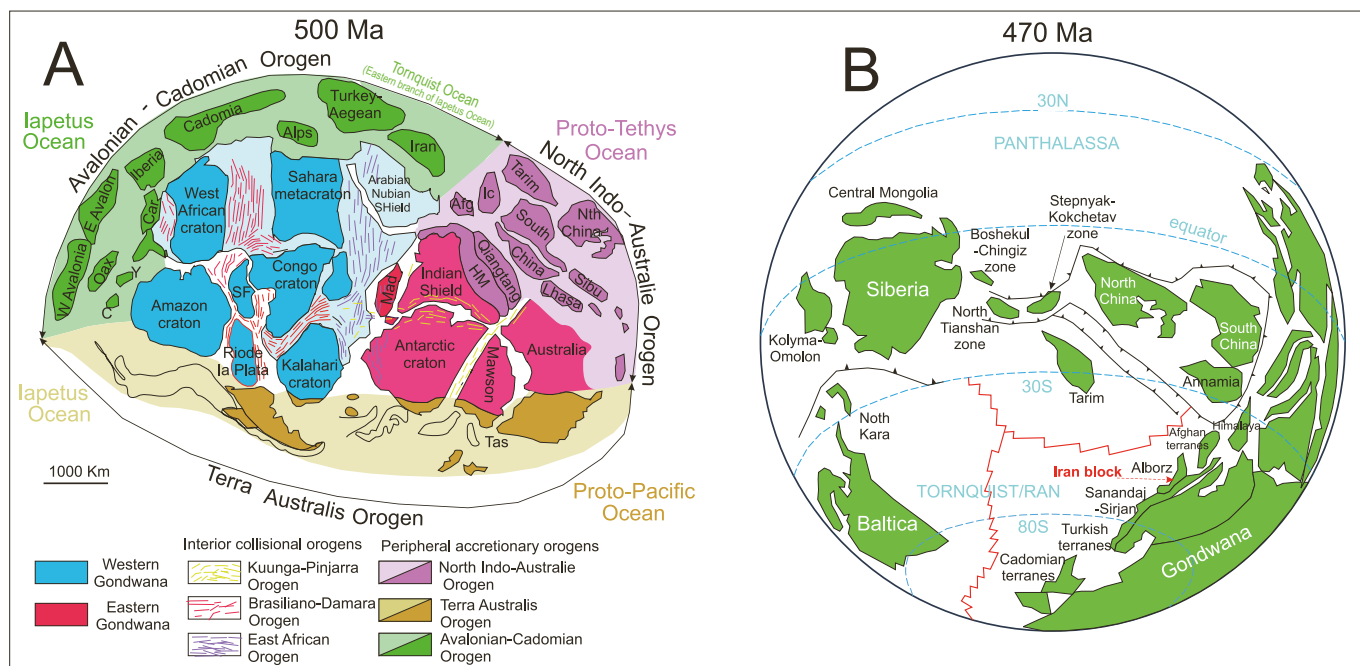


Fig. 1. (A) Map of Gondwana at ca. 500 Ma showing cratonic blocks and interior and peripheral orogens. The absolute and relative positions of most blocks within the peripheral orogens are poorly constrained and positions depicted on this diagram are indicative only. (B) Paleogeographic plate model at 470 Ma showing the general situation along the Gondwanan margin (right side). The different perspective on the left illustrates the relationships between Laurentia, Baltica, Gondwana and the intervening Rheic and Iapetus oceans (from Domeier 2016, 2017). Abbreviations: Afg – Afghanistan; C – Cortis; Car – Carolina; CC – Cuyania and Chilenia; FL – Florida; IC – Indochina; HM – Himalayas; Mad – Madagascar; Oax – Oaxaquia; SF – San Francisco; Tas – Tasmania; WDF – Western Deformational Front; Y – Yucatan.

provide an insight in a transect across the Cadomian active margin, which comprise mafic and felsic igneous rocks and associated sedimentary successions. They have geochemical compositions consistent with an extensional, rifted basin environment. Their deposition most likely occurred in a poorly developed, limited, and irregularly subsiding passive-margin (Moghadam et al., 2017). Paleozoic successions are documented in the Sotori Mountains (Ashouri, 2002), Djam region (Alavi-Naini, 1972), Torud area (Hushmandzadeh et al., 1978), Shirgesht area (Ghasemi and Derakhshi, 2008), Gorgan Schists (Ghavidel-Syook, 2008), Kuh-e-Kharbash basalts (Mehdizadeh Shahri, 2008), Abyane-Soh area (Ayati et al., 2011), Soltan Maidan Basalts (Derakhshi and Ghasemi, 2015, Derakhshi et al., 2017), Jalal Abad mafic rocks (Vesali et al., 2020) and Maku area (Valinasab Zarnagh et al., 2021) (see red stars in Fig. 2A).

An incomplete and spatially variable Silurian–Carboniferous section across Iran suggests periods of non-deposition and erosion (e.g., Wendt et al., 2005). In spite of lithological and lithostratigraphic similarities, Paleozoic clastic units and igneous rocks in northern Iran (Alborz Mountain Ranges and Kopeh Dagh) and central Iran have different names (Fig. 3). For northern Iran, these include the late Ordovician Qelli Formation, and the early Devonian Soltan Meidan basalts and the Padeha Formation (Wendt et al., 2005). The central Iran clastic units include the Early Ordovician Shirgesht, the Silurian Niur and the Early Devonian Padeha formations (Fig. 3).

Eiacaran to Late Paleozoic magmatic-sedimentary sequences (>4 km thick) in northern Iran are exposed over >600 km along the Alborz Mountain Ranges, from Zanjan in the west to Binaloud in the east (Fig. 2A–B). The Alborz Mountain Ranges was part of the southern passive margin of Gondwana (e.g., Wendt et al., 2005; Ghavidel-Syooki, 2008; Moghadam et al., 2017) and was accreted to Eurasia as the result of the closure of the Paleotethys in Late Triassic (Berberian and King, 1981). Further east, the eastern Alborz magmatic-sedimentary successions merge with their equivalents in the Kopet Dagh zone, which have the same ages, but correspond to different depositional environments (Berberian and King, 1981).

The Binaloud zone is a linear, nearly NW-oriented magmatic-sedimentary belt (Fig. 4). It is located at the east of the Alborz Mountain Ranges and west of the Paropamisus Mountains in northern Afghanistan, south of Mashhad-Quchan and north of Neyshabur-Sabzevar. This zone represents a gradual transition of the Alborz and Central Iranian zones, between the Turan block of Laurasia in the northeast and the Central Iranian microcontinent in the southwest, that developed during the Cimmerian and Alpine orogenies (Stöcklin, 1968). It dominantly comprises Paleozoic volcano-sedimentary successions that formed after the Cadomian Orogeny at 500–480 Ma (e.g., Topuz et al., 2018). Some of the volcano-sedimentary sequences preserve a diversity of volcanic rocks of different ages that provide useful information on their geotectonic settings and thus on the geologically plausible tectonic evolution of the area in the eastern margin of the Avalonian-Cadomian Orogenic belt (Moghadam et al., 2017; Fig. 1C).

2.1. Local geology and field observations

The Binaloud zone comprises large volumes of up to 1200 m thick basaltic lava flows along with interlayered coarse- and fine-grained gabbroic rocks that are exposed in the tuff, agglomerate, sandy limestone and sandstone (Fig. 4). They are accompanied by a few 10 to 20 cm thin sedimentary interlayers of shale, siltstone, sandstone and conglomerate. This complex is composed of both subaerial and submarine environments (Topuz et al., 2018). The contacts between the studied magmatic and metasedimentary rocks are sharp (Fig. 5A). The best preserved and most complete outcrop of the Binaloud zone occurs in the Buzhan and Baghroud regions, where the studied mafic rocks are gray to dark green and fine- to medium-grained with no or only a very weak foliation. The study area includes Paleozoic, Mesozoic and Cenozoic rocks. There are no exposures of Early Ordovician strata of the Qelli

formation, which is consistent with periods of non-deposition and erosion in this region (e.g., Wendt et al., 2005). The Late Ordovician–Silurian strata are characterized by abundant sandstone, carbonate and shale that are overlain and intruded by abundant massive and pillow basaltic and gabbroic rocks. These igneous rocks are interpreted as equivalents of the Late Ordovician–Silurian Soltan–Meidan Formation (Aharipour et al., 2009; Figs. 3 and 4).

The Paleozoic units of the Binaloud Zone (Fig. 4) are composed of Early Cambrian, slightly metamorphosed sedimentary rocks (Mila formation) along with Silurian–Devonian sedimentary rocks (the 300 m thick Padeha, the Sibzar, and the 200 m thick Bahram formations), Silurian volcanic rocks interlayered with fine- and coarse-grained gabbro, agglomerate, tuff, and several Devonian mafic sills and dikes (Figs. 4 and 5A–C). The relatively continuous and alternating outcrops of the basaltic and fine- and coarse-grained subvolcanic gabbroic rocks can be traced over a length of about 40 km along the Binaloud zone (Fig. 5A), which constrains the roughly same ages for all these rocks. The original thicknesses of the volcanic and subvolcanic fine- and coarse-grained gabbroic successions are uncertain due to subsequent tectonic events, the mountainous condition of the area and also the steep slopes of the valleys. Our field work indicates that their present thickness reaches to ca. 300 m. Field relations show that unknown amounts of the original volcanic rocks have been eroded and weathered prior to the deposition of the Silurian Niur Formation. These Late Ordovician–Silurian strata are, along with conglomerate and siliciclastic rocks (~10 m) part of the base of the section (Ghavidel-Syooki et al., 2011), where they are juxtaposed to the Mila Formation along a faulted contact (Fig. 5A–B). The Niur Formation in our study area is a thin and discontinuous unit, consisting of thin layers of shale and sandstone interbedded with fossiliferous limestone. In this region, the mafic rocks of the Late Ordovician–Silurian of Binaloud are interpreted to be conformably underlain by the ~300 m thick Padeha Formation. The Padeha Formation preserves evidence of Devonian uplift and erosion followed by marine transgression (Fig. 4; Aharipour et al., 2009). This formation is subdivided into three members. The lowest member has a variable thickness up to 10 m and mainly consists of red conglomerate, which contains abundant pebble- to boulder-sized (3–50 cm) igneous and sedimentary clasts. Red siltstone, green tuff and interlayers of basaltic to andesitic massive and pillowed lava are also common between the conglomerate layers. Locally-derived boulders of A-type granite are an important clast type with an age of 441.0 ± 3.1 Ma based on a zircon U–Pb concordia (Moghadam et al., 2017). The intermediate member contains white-coloured quartz–arenite that rests on basaltic lava of the lowest member, where the two are clearly unconformable. Alternating quartz–arenite, arkosic sandstone, and greywacke with red shale are also common in the intermediate member. The upper member is characterized by carbonate layers and fine-grained siliciclastic rocks and red to green shale. The carbonate rocks consist of abundant yellowish calccrete and dolocrete. The Padeha Formation is overlain by the Khosh Yeylugh limestone and red sandstone. Palynological data yielded Late Devonian ages for both formations (Ghavidel-Syook, 2008).

2.2. Sample description and petrography

The Binaloud magmatic rocks are composed of dark gray coarse- and fine-grained gabbro, which are interlayered with mafic volcanic rocks. The lavas are characterized by ophitic, vitritic and porphyritic textures (Fig. 5D–F) and include basalt and basaltic andesite. Phenocrysts include plagioclase (up to 25%) and augite (up to 10%) and are set in a groundmass of plagioclase, augite, and Fe–Ti oxides (Fig. 5D). Relic olivine is also present in a few samples, but it has been mainly replaced by secondary minerals. Based on decreasing order of abundance, the Fe–Ti oxides in the investigated rocks include magnetite, ilmenite and titanomagnetite. Alteration is a widespread process in the studied rocks, so that minerals such as chlorite, calcite, epidote, quartz, albite, titanite, and clay minerals are common. Electron microprobe analyses (EMPA) of

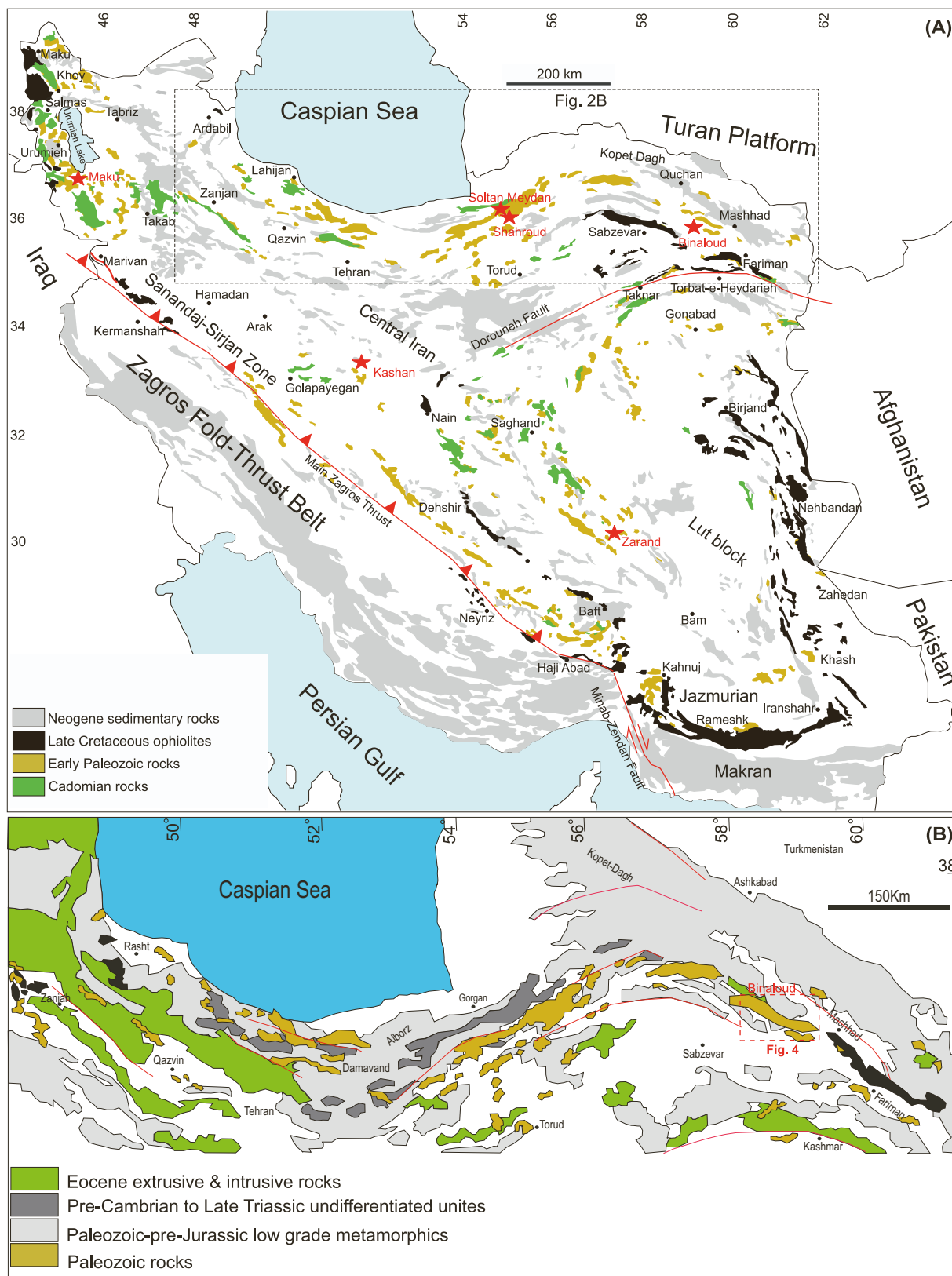


Fig. 2. (A–B) Distribution of Neoproterozoic–Paleozoic sedimentary and igneous rocks in Iran (modified after 1/1000000 Geological Map of Iran, GSI) showing the location of Binaloud in the NE Iran.

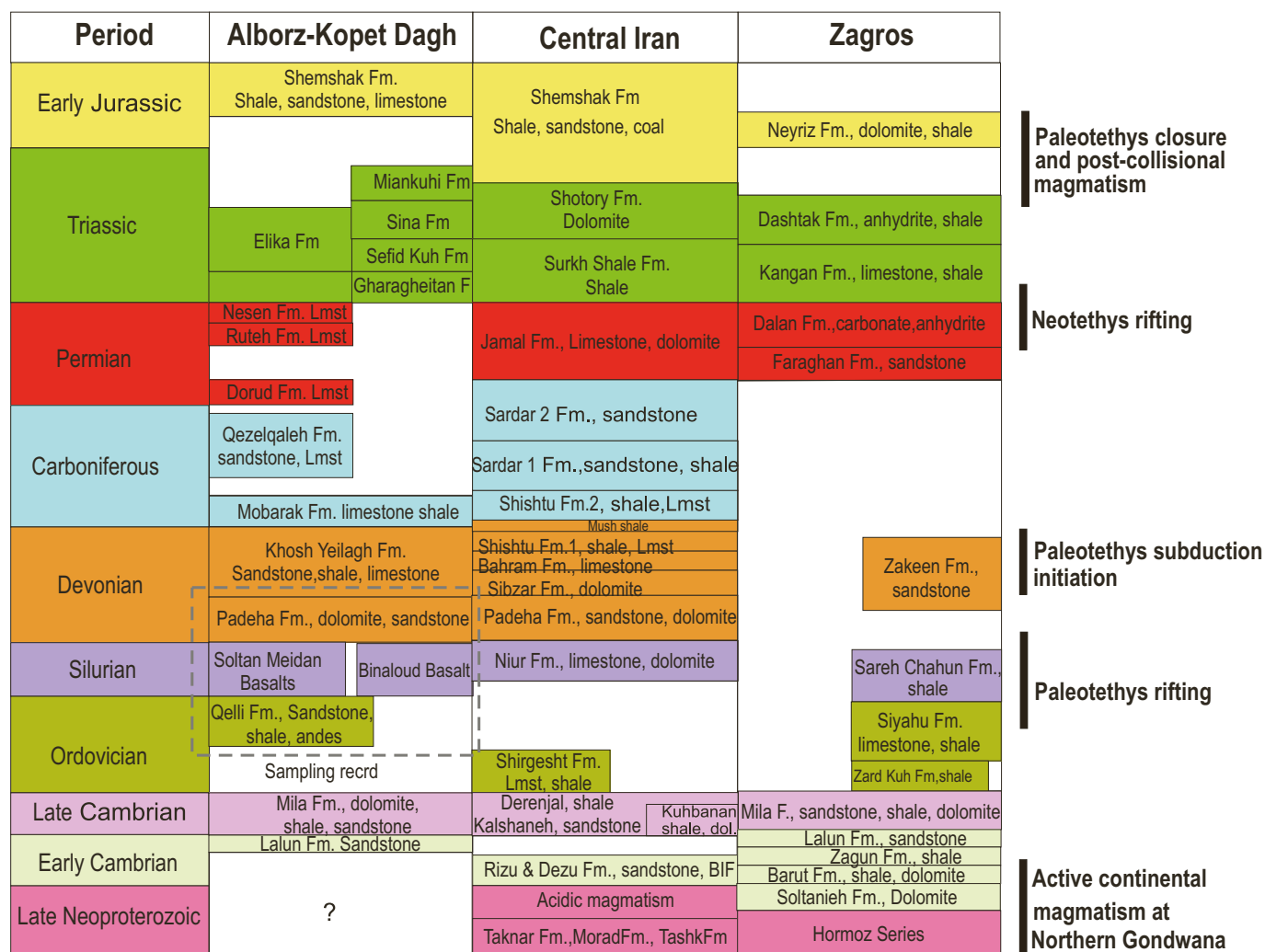


Fig. 3. Stratigraphic chart of Iran for Eastern Alborz, central Iran and Zagros zones from Neoproterozoic to Jurassic (Modified after Moghadam et al., 2017).

plagioclase indicate extensive replacement of labradorite by albite (see next section; Fig. 6B). The fine-grained gabbro is characterized by microgranular (Fig. 5G) and ophitic (Fig. 5H) textures consisting of clinopyroxene (45–55 vol%), plagioclase (30–40 vol%), Fe–Ti oxides (~10 vol%), and apatite (~5 vol%), with subsidiary zircon. Clinopyroxene has been partly replaced by chlorite. The coarse-grained gabbro, which is characterized by granular and ophitic textures (Fig. 5I), includes the same mineralogy of clinopyroxene (40–45 vol%), euhedral to subhedral plagioclase (50–55 vol%), Fe–Ti oxides (~5 vol%), and subsidiary apatite and zircon (Fig. 5I). Plagioclase is partly included in clinopyroxene. Clinopyroxene is partly replaced by amphibole and chlorite, except for some samples, in which clinopyroxene is present as inclusions within secondary minerals.

3. Analytical methods

Compositions of clinopyroxene and plagioclase were determined at the Wuhan Technology University of China (WTU), Wuhan, using a JEOL JXA-8230 electron microprobe. The accelerating voltage was ~30 kV and the beam current was 10⁻⁵ ~ 10⁻¹² nA. Probe determinations are accurate within 0.02 wt% for Si, Al and K, 0.03 wt% for Ti, Mg, Ca and Na, 0.07 wt% for Fe, 0.08 wt% for Mn and 0.11 wt% for Ni. Data were revised using a modified ZAF (atomic number, absorption, fluorescence) correction procedure.

Whole-rock geochemical analyses for representative unaltered or least-altered samples were performed at the Wuhan Sample Solution

Analytical Technology Co., Ltd., Wuhan, China, after crushing all the selected samples to powder of <200 mesh. Major element concentrations were determined by X-ray fluorescence (XRF). The measurement procedure and data quality were monitored by simultaneous analyses of repeated samples (one in ten samples) and the standard samples GBW07103, GBW07105, GBW07110, GBW07111, and GBW07112. The analytical uncertainties are generally <1% for most major elements. Trace element (including rare earth element) concentrations were determined by an Agilent 7700e ICP-MS. The compositions of repeated samples (one in ten samples) and the reference materials AGV-2, BHVO-2, BCR-2, and RGM-2 were also analyzed to monitor the data quality. The analytical uncertainties are better than 5% for most trace elements. The detailed analytical procedures are the same as those described by Liu et al. (2008).

Strontium–Neodymium isotopic compositions were analyzed by a multiple collector inductively coupled plasma mass spectrometry (Neptune Plus MC-ICP-MS) at the Wuhan Sample Solution Analytical Technology Co., Ltd., Wuhan, China. Details of the analytical procedures are given in Lin and Fraser (2003). The measured Sr and Nd isotope ratios were normalized to ⁸⁸Sr/⁸⁶Sr = 8.375209 and ¹⁴⁶Nd/¹⁴⁴Nd = 0.7219, respectively. During the analyses, the BCR-2 standard yielded a ⁸⁷Sr/⁸⁶Sr ratio of 0.705007 ± 10 (2σ) and a ¹⁴⁶Nd/¹⁴⁴Nd ratio of 0.512642 ± 7 (2σ), which were identical within an error to the previously reported values.

U–Pb dating and trace element analyses of zircon were conducted synchronously by LA-ICP-MS at the Key Laboratory for the study of

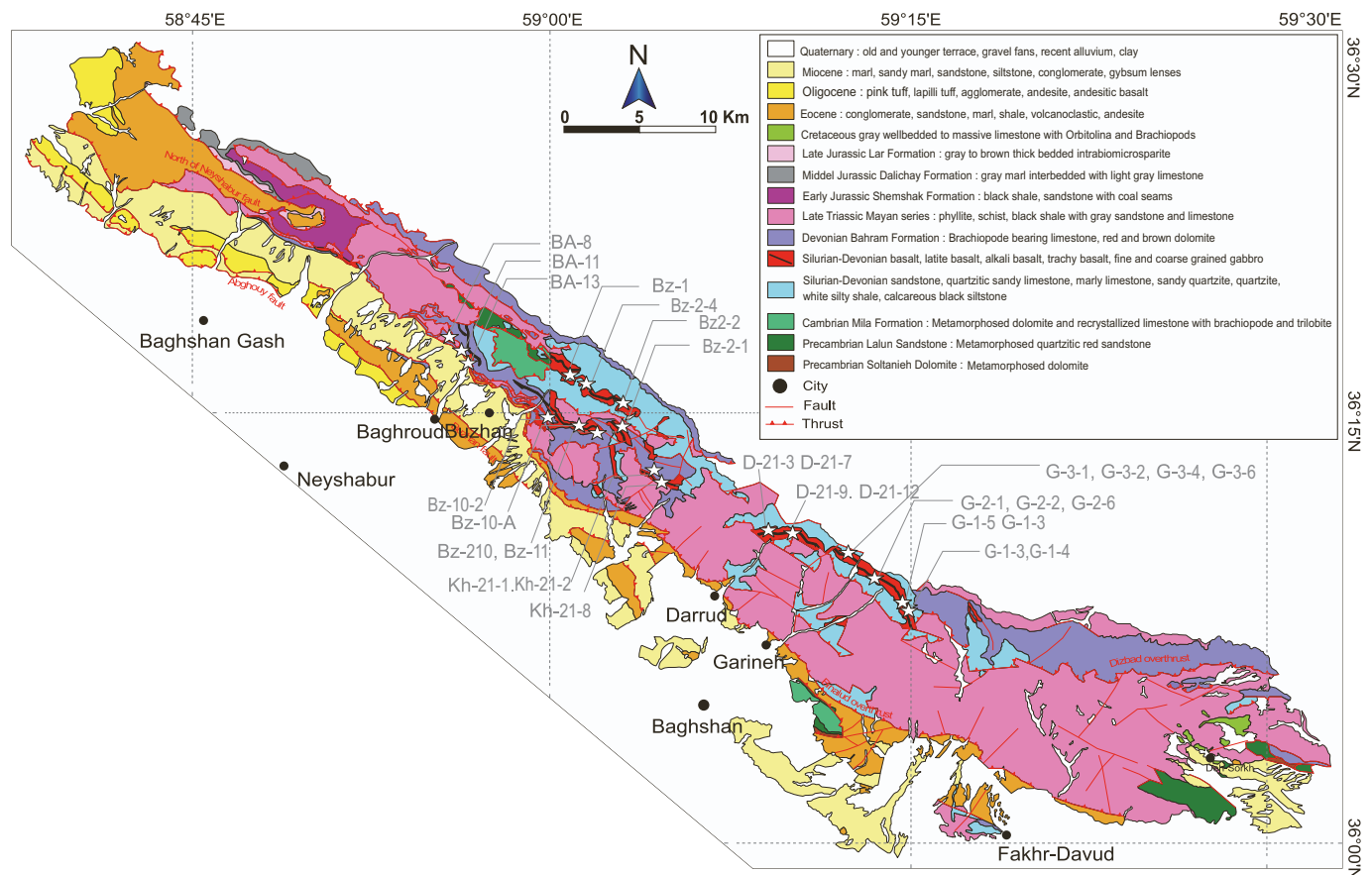


Fig. 4. Geological map Binaloud region (modified after Geological map of Mashhad and Neyshabour, GSI) showing the sedimentary and igneous units relationships and sampling units.

focused Magmatism and Giant ore Deposits, MNR, Xi'an Center of Geological Survey (CGS). Laser sampling was performed using a GeoLas Pro. An Agilent 7700× ICP-MS instrument was used to acquire ionic intensities. Helium was applied as a carrier gas. Argon was used as the make-up gas and mixed with the carrier gas via a T-connector before entering the ICP. Each analysis incorporated a background acquisition of approximately 10 s (gas blank) followed by 40 s data acquisition from the sample. The Agilent Chemstation was utilized for the acquisition of each individual analysis. Off-line selection and integration of background and analyte signals, and time-drift correction and quantitative calibration for trace element analyses and U–Pb dating were performed by Glitter 4.4. Details of the instrumental conditions and data acquisition procedures are similar to those described by Li et al. (2015). Zircon 91,500 and GJ-1 were used as external calibration standards and the standard silicate glass NIST 610 was used to optimize the machine. Time-dependent drifts of U–Th–Pb isotopic ratios were corrected using a linear interpolation (with time). Uncertainty of preferred values for the external standard 91,500 was propagated to the ultimate results of the samples. Concordia diagrams and weighted mean calculations were made using Isoplot/Ex ver 3 (Ludwig, 2003). Trace element compositions of zircons were calibrated against reference materials (NIST610) combined with Si as internal standardization. The preferred values of element concentrations for the NIST reference glasses are from the GeoReM database (<http://georem.mpch-mainz.gwdg.de/>).

4. Results

4.1. Mineral compositions

Mineral chemistry of representative clinopyroxene and plagioclase from fine- to coarse-grained gabbro and basalt samples are given in the Supplementary Table S1 and are plotted in the Wo–En–Fs (Fig. 6A) and An–Ab–Or (Fig. 6B) ternary diagrams, respectively.

The analyzed clinopyroxene grains are dominantly augite with minor diopside ($Wo_{42-44}En_{36-39}Fs_{16-21}$ and $Wo_{41-45}En_{28-38}Fs_{16-29}$ in the fine- and coarse-grained gabbro, respectively; Fig. 6A). Clinopyroxene of the fine-grained gabbro is characterized by SiO_2 concentrations of 49.6 to 51.3 wt%, TiO_2 from 1.5 to 2.5 wt%, Al_2O_3 from 2.6 to 3.5 wt%, FeO_T from 10.5 to 11.6 wt%, MgO from 12.5 to 13.3 wt%, CaO from 19.5 to 20.5 wt%, and Na_2O from 0.4 to 0.7 wt%, with $Mg\#$ (100 $Mg/(Mg + Fe)$ molar) ranging from 64.3 to 67.3. Clinopyroxene of the coarse-grained gabbro has a limited range of SiO_2 concentrations (49.5–51.3 wt%), similar CaO (19.5–21.1 wt%), lower TiO_2 (0.6–1.2 wt%), Al_2O_3 (1.2–3.1 wt%), MgO (9.8–13.3 wt%) ($Mg\# = 61.0-64$), and Na_2O (0.25–0.82 wt%), and higher FeO_T (10.5–16.3 wt%) concentrations compared with those of the fine-grained gabbro. Clinopyroxene grains from the coarse-grained gabbro have reverse compositional zoning, characterized by decreasing MgO concentrations, and $Mg\#$ from core to rim (Fig. 6C; Supplementary Table S1). By contrast, clinopyroxene from the fine-grained gabbro has generally normal compositional zoning with decreasing MgO concentrations and $Mg\#$ from core to rim (Fig. 6D; Supplementary Table S1).

Clinopyroxene from basalt is mainly augite ($Wo_{34-45}En_{38-50}Fs_{6-23}$) and characterized by SiO_2 concentrations of 51.1 to 53.3 wt%, TiO_2 from 0.22 to 1.04 wt%, Al_2O_3 from 1.1 to 2.7 wt%, FeO_T from 4 to 15 wt%,

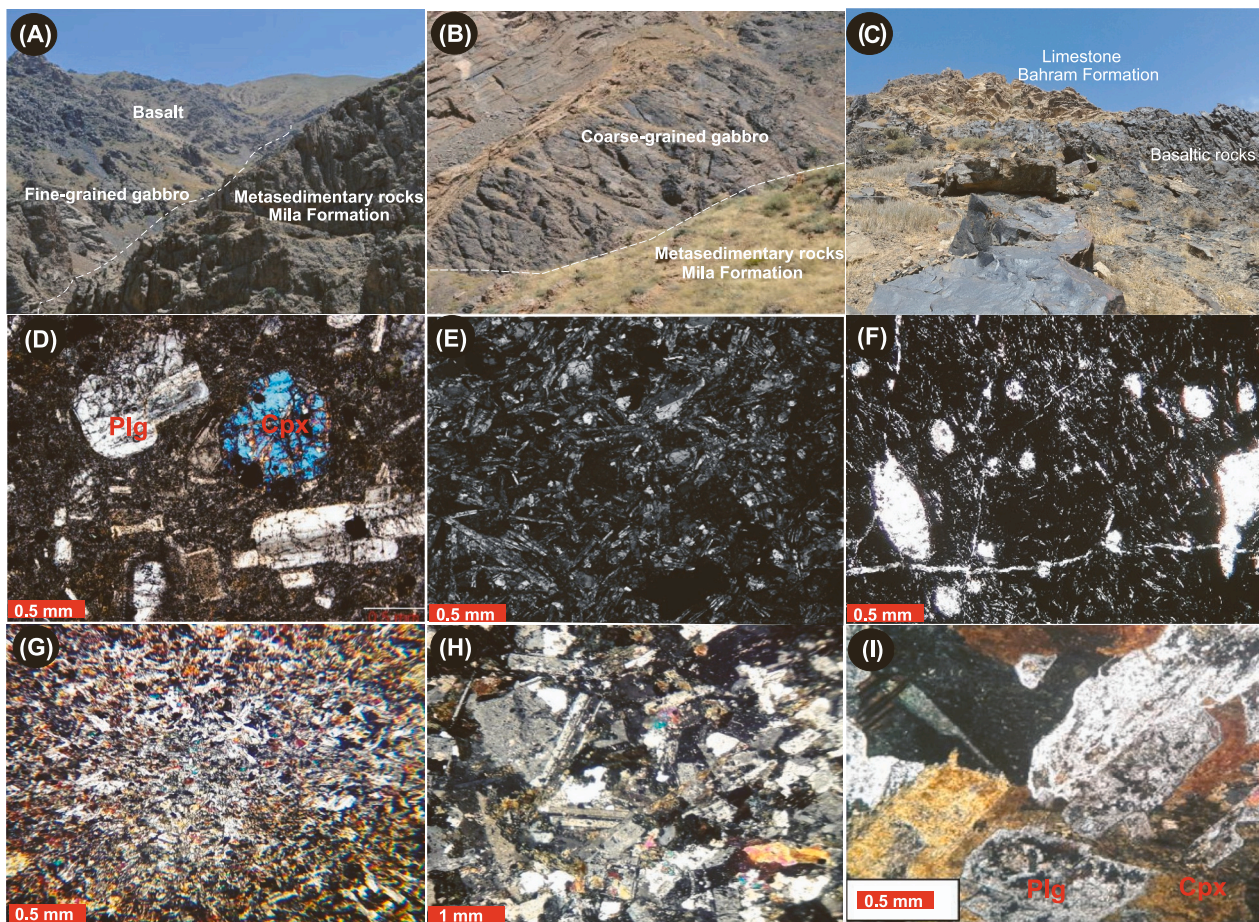


Fig. 5. (A–C) Field photos showing occurrences of (A) microgabbro and basalts with faulted contact with Mila formation; (B) Coarse-grained gabbro and meta-sedimentary rocks of Mila formation; (C) Basalts conformably covered with Devonian limestone of Bahram formation in the Binaloud zone. (D–I) Photomicrographs of gabbro and basalts in the Binaloud zone. (D) Phenocrysts of plagioclase and augite in porphyritic Basalt (cross-polarized light); (E) Subophitic texture of basalt (cross-polarized light); (F) Microcrystalline and vitric basalt (cross-polarized light); (G) Microgranular texture of fine-grained gabbro (cross-polarized light); (H) Fine-grained gabbro with subophitic texture (cross-polarized light); (I) Coarse-grained gabbro with granular, ophitic and poikilitic textures. Cpx: clinopyroxene; Plg: plagioclase.

MgO from 13.4 to 17.8 wt%, CaO from 19.69 to 21.12 wt%, and Na₂O from 0.41 to 0.61 wt%, with Mg# ranging from 61 to 88.

The composition of Binaloud basalt, fine- and coarse-grained gabbro clinopyroxene also indicates an alkaline affinity of their parental melts (Fig. 6E). Clinopyroxene is also an important mineral for identifying tectonic settings. On the F1 vs. F2 diagram, the samples of this study indicate an intracontinental environment (Supplementary Table S1; Fig. 6F).

Plagioclase from the coarse-grained gabbro has anorthite compositions ranging from 43 to 65, and plot in the labradorite field (Fig. 6B; Supplementary Table S2b), with SiO₂, Al₂O₃, CaO and Na₂O in the range of 51.3 to 55.3 wt%, 25.7 to 29.9 wt% and 9.2 to 13.5 wt% and 3.2 to 5.5 wt%, respectively. One analysis of a plagioclase rim yielded lower An concentrations (43), and plots within the andesine field (Fig. 6B). Fresh plagioclase in basalt is characterized by the same composition as those in coarse-grained gabbro. It is characterized by labradorite composition with SiO₂, Al₂O₃, CaO and Na₂O in range of 51.4 to 54.1 wt %, 28.0 to 29.6 wt% and 11.7 to 13.0 wt% 4.3 to 4.8 wt%, respectively. Conversely, altered plagioclase has a more sodic composition (An contents up to 3) and plots in the albite field (Fig. 6B).

4.2. Major and trace element whole-rock compositions

Major and trace element compositions of the studied Binaloud basalt are given in the Supplementary Table S2. All of the analyzed samples

exhibit narrow compositional ranges. SiO₂ contents of basalt ranges from 44.0 to 49 wt%, TiO₂ from 1.9 to 4.3 wt%, Al₂O₃ from 12 to 17 wt %, Fe₂O₃ from 13.3 to 18.9 wt%, MgO from 3.5 to 8.7 wt%, Na₂O from 2.6 to 5.2 wt%, K₂O from 0.2 to 1.9 wt%, and Mg# from 30 to 60 with mean at 41. In Zr/TiO₂ vs. Nb/Y (Winchester and Floyd, 1977) and TiO₂ vs. Nb/Y diagrams (Fig. 7A, B), the sample data fall in the field of alkaline basalt. Their Cr and Ni concentrations range from 10 to 110 ppm and from 21 to 191 ppm, respectively. All the samples are enriched in large ion lithophile elements (LILEs; e.g., Cs, Ba) and high-field strength elements (HFSEs; e.g., Nb), and negative Yb anomalies in the primitive mantle-normalized trace-element spider diagram (Fig. 8B). Overall, the total REE concentrations and trace element patterns of the basalt, together with those of other early Paleozoic alkaline rocks throughout Iran, are similar to those of intraplate extensional basin OIBs (Sun and McDonough, 1989; Fig. 8A). Total REE contents (ΣREEs) of the samples vary from 94 to 282 ppm, with a mean of 175 ppm, which is slightly lower than the average OIB value (199 ppm; Sun and McDonough, 1989). In the chondrite-normalized REE diagram (Fig. 8A), the basalt samples exhibit an enrichment in light REEs (LREEs), with (La/Yb)_N ratios of 4.1–19.9 (mean of 8.9) and Eu/Eu* ratios of 0.8 to 1.2 (mean of 1.03).

The fine-grained gabbro has concentrations of SiO₂ of 47.8 to 48.9 wt %, MgO of 3.7 to 5.6 wt%, CaO of 5.3 to 6.5 wt%, TiO₂ of 2.6 to 2.8 wt%, and P₂O₅ of 0.3 to 0.6 wt%, with Mg# of 30 to 33. The coarse-grained

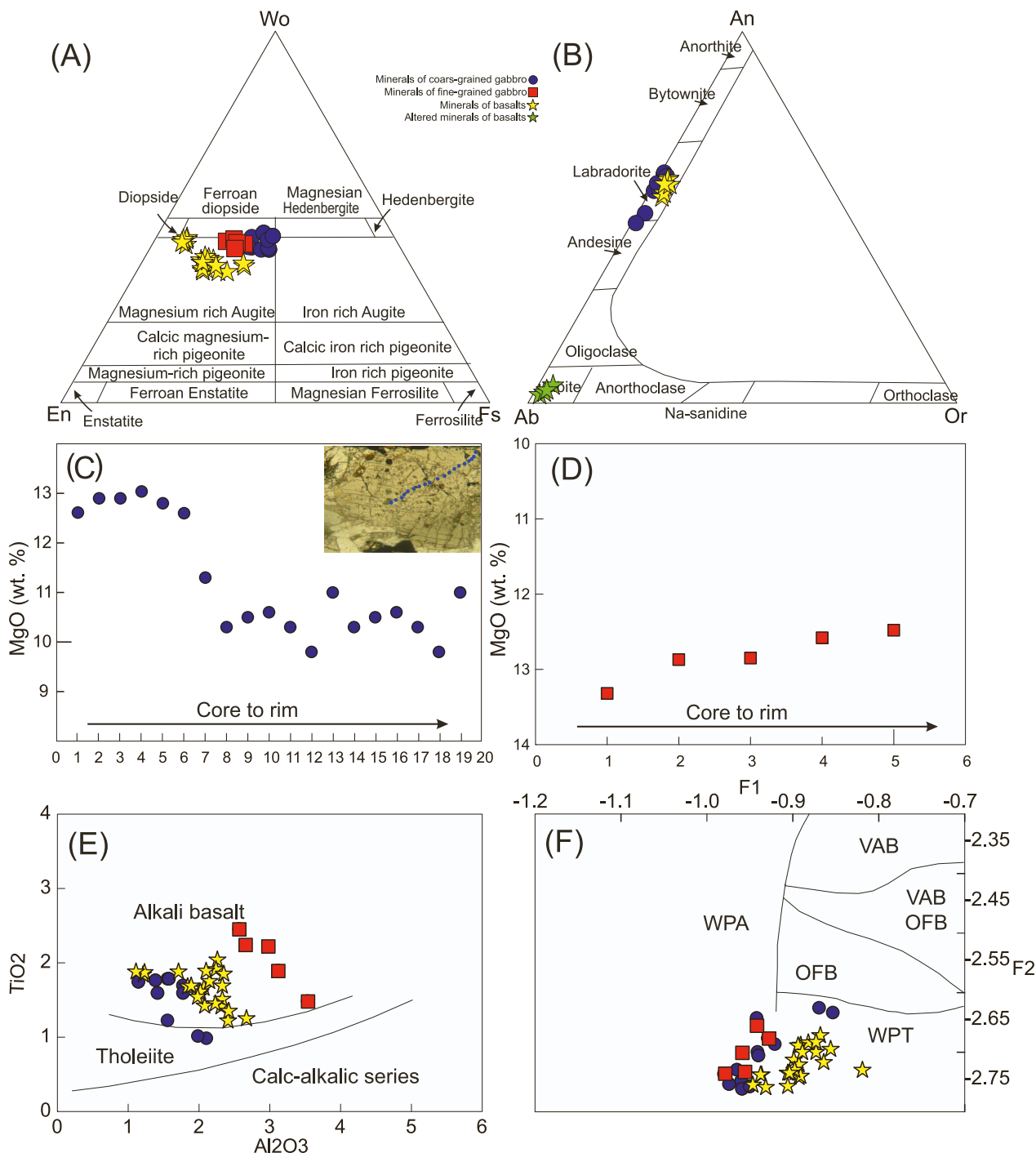


Fig. 6. Ternary classification diagrams for (A) Ca-Mg-Fe pyroxenes (Rock, 1990) and (B) feldspars (Smith and Brown, 1988); (C) representative clinopyroxene grain in the Coarse-grained gabbro sample and its compositional variations; (D) representative clinopyroxene grains in the fine-grained gabbro sample and their compositional variations. $F1 = (-0.012 * SiO_2) - (0.0807 * TiO_2) + (0.0026 * Al_2O_3) - (0.0012 * FeOt) - (0.0026 * MnO) + (0.0087 * MgO) - (0.0128 * CaO) - (0.0419 * Na_2O)$; $F2 = (-0.0469 * SiO_2) - (0.0818 * TiO_2) + (0.0212 * Al_2O_3) - (0.0041 * FeOt) - (0.1435 * MnO) + (0.0029 * MgO) - (0.0085 * CaO) - (0.016 * Na_2O)$. Cpx = clinopyroxene; Pl = plagioclase.

gabbro is characterized by concentrations of SiO_2 of 48.5 to 52.6 wt%, MgO of 2.2 to 3.6 wt%, CaO of 4.2 to 6.5 wt%, TiO_2 of 1.8 to 2.8 wt%, and P_2O_5 of 0.28 to 0.65 wt%, with Mg# of 34 to 49. Both coarse- and fine-grained gabbros are characterized by Cr and Ni concentrations of 14.7 to 60.5 ppm and from 11.5 to 88 ppm, respectively, and an enrichment in Nb (23.7–52.7 ppm) and Ta (1.5–3.3 ppm).

In the Zr/TiO_2 vs. Nb/Y (Winchester and Floyd, 1977) and TiO_2 vs. Nb/Y (Fig. 7B) diagrams, coarse- and fine-grained gabbros plot in the alkaline basalt fields, respectively. Total REE concentrations ($\Sigma REEs$)

vary from 82 to 287 ppm, with a mean of 160 ppm, which is slightly lower than the average OIB value (199 ppm; Sun and McDonough, 1989). The gabbro is also enriched in LREEs, with $(La/Yb)_N$ ratios of 3.8–8.9 (mean of 6.5) and Eu/Eu^* ratios of 0.9 to 1.1 (mean of 1.00) and an absence of negative Eu anomalies (Fig. 8C). In the primitive mantle-normalized trace-element spider diagram (Fig. 8D), the studied gabbro displays an enrichment in LILEs and HFSEs, and positive U and Yb anomalies. Overall, the trace element patterns of the gabbro have transitional trace element characteristics between OIBs and enriched

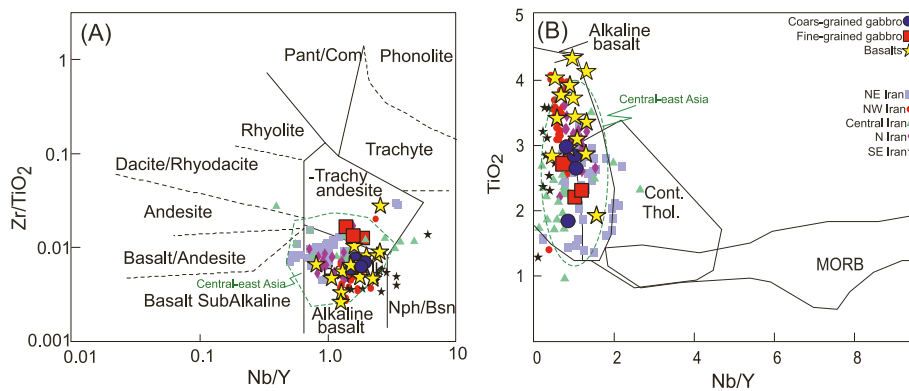


Fig. 7. (A) Zr/TiO₂ versus Nb/Y (Winchester and Floyd, 1977) and (B) TiO₂ versus Nb/Y diagrams (Winchester and Floyd, 1976). Data sources for Early Paleozoic mafic rocks come from in the NE (Soltan Meidan: Derakhshi et al., 2017), NW (Maku: Valinasab Zarnagh et al., 2021), central (Bafq: Niktabar and Rashidnejad Omran, 2016; Ardakan: Nouri et al., 2022), SE (Zarand: Vesali et al., 2020).

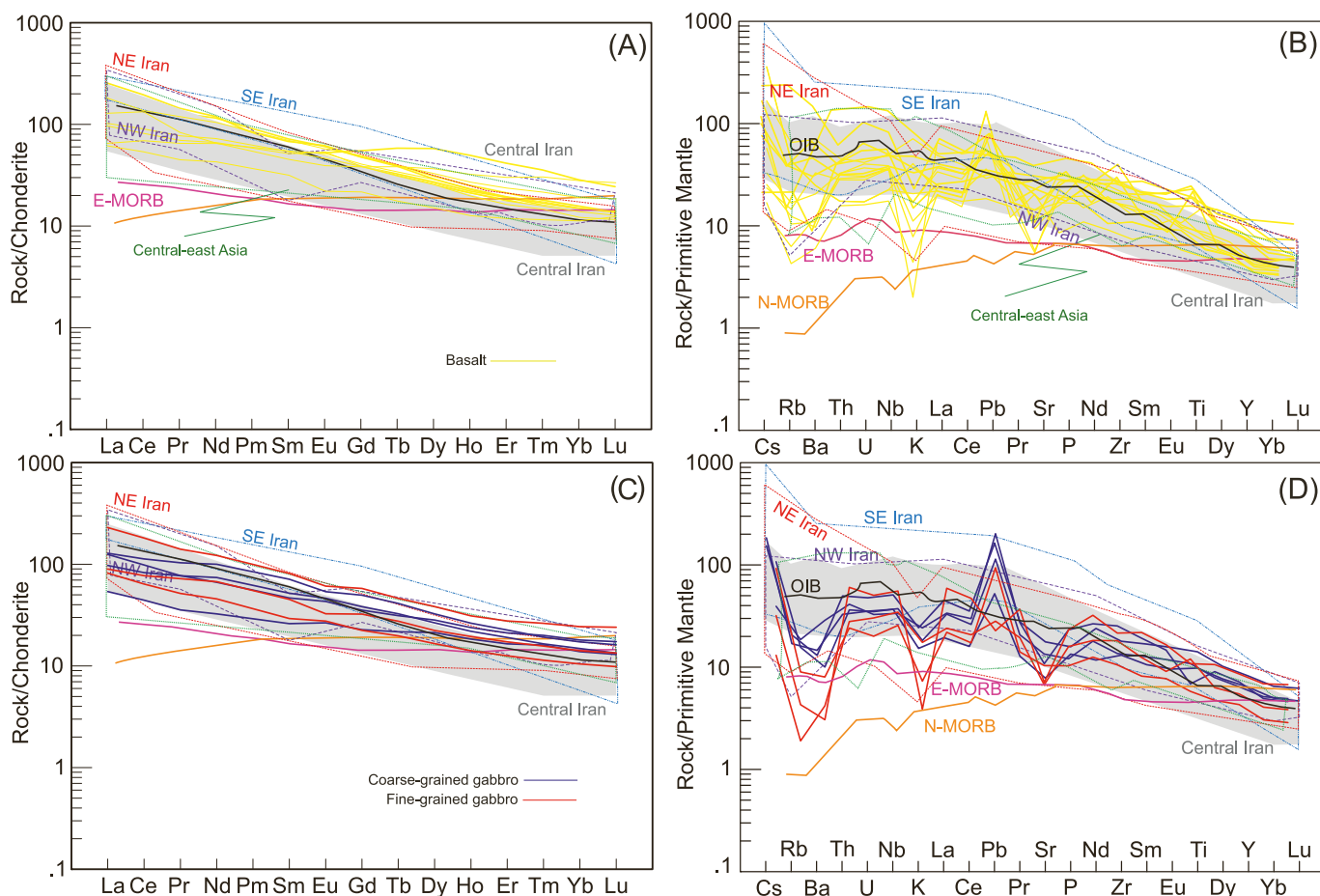


Fig. 8. (A and C) Chondrite-normalized REE patterns of basalt and gabbro samples respectively, and (B and D) primitive mantle-normalized trace element spider diagrams of same rocks. Chondrite and primitive mantle normalized values are from Sun and McDonough (1989). Data sources as same with Fig. 7.

mid-ocean ridge basalts (E-MORBs; Sun and McDonough, 1989; Fig. 8D).

4.3. Strontium and neodymium isotopes

Strontium and neodymium isotope abundances and ratios of the Binaloud rocks are given in the Supplementary Table S3. All initial isotope ratios, on the basis of the obtained ages of this study (see Section 4.4), are corrected. The studied basalt samples of Binaloud have initial ⁸⁷Sr/⁸⁶Sr ratios ranging from 0.70501 to 0.70570, except one sample

with more a radiogenic value of 0.70911, ¹⁴³Nd/¹⁴⁴Nd ranging from 0.51209 to 0.51225 and εNd = +0.1 to +3.2 (Fig. 9; Supplementary Table S3). The Binaloud fine- and coarse-grained gabbro has relatively uniform Sr and Nd isotopic compositions, with initial ⁸⁷Sr/⁸⁶Sr ratios of 0.70717–0.70727, εNd(t) of +1.2 to +1.8, and depleted mantle Nd model ages (TDM) ranging from 1.1 to 1.5 Ga. The Nd and Sr isotopic compositions of the Binaloud basalt are similar to those of rocks from Soltan Meidan, Alborz (⁸⁷Sr/⁸⁶Sr of 0.704138 to 0.706733, ¹⁴³Nd/¹⁴⁴Nd of 0.512440 to 0.512746, ⁸⁷Sr/⁸⁶Sr_{initial} = 0.704062–0.705697, ¹⁴³Nd/¹⁴⁴Nd_{initial} = 0.512064–0.512315, εNd(t) = –3.86 to +2.10;

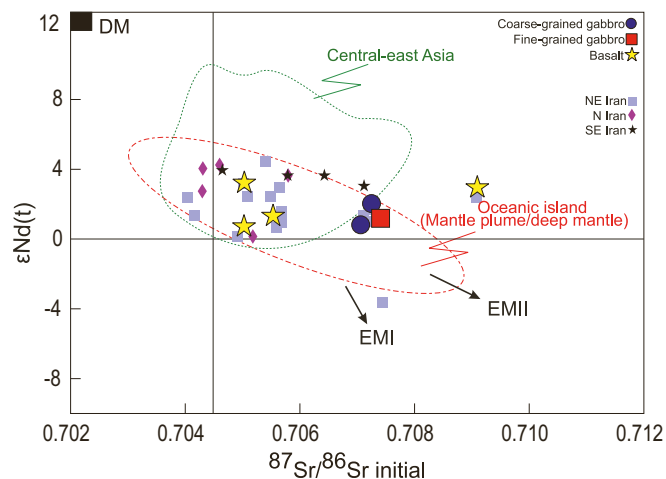


Fig. 9. $\epsilon Nd(t)$ versus ISr diagram. Data sources in N-MORB, OIB- and E-MORB-like rocks from Safonova et al., 2016. Data sources as same with Fig. 7.

Derakhshi et al., 2017), and the mafic rocks of Zarand, SE Iran ($^{87}Sr/^{86}Sr_{initial} = 0.704138\text{--}0.706733$, $^{143}Nd/^{144}Nd_{initial} = 0.5124$ to 0.5126 with $\epsilon Nd(i)$ ranging from -1.43 to $+1.50$; Vesali et al., 2020). However, the related gabbro is characterized by more radiogenic $^{87}Sr/^{86}Sr_{initial}$ ratios with respect to the Binaloud, Soltan Meidan and Zarand basalt (Fig. 9).

4.4. Geochronology

One coarse-grained gabbro sample (Gb-2-1) and one fine-grained gabbro sample were selected for LA-ICP-MS U–Pb zircon dating, and the results are presented in the Supplementary Table S4 and plotted on the concordia diagram (Fig. 10). Representative cathodoluminescence (CL) images are shown in Fig. 10a. The zircon grains are mostly semi-transparent, euhedral to subhedral, and have short prismatic shapes,

with a crystal length to width ratio of 1:1 to 3: 1. Most zircons grain show oscillatory zoning in CL images (Fig. 10), consistent with the typical characteristic of igneous zircons of mafic rocks (Rubatto and Gebauer, 2000). Sixteen analyses from the coarse-grained gabbro were obtained from 16 grains, which have variable U (452–3592 ppm) and Th (474–7951 ppm) concentrations, with high Th/U ratios of 0.8–4.2. Six analyses yielded high U (1399–3592 ppm), Th (1976–7951 ppm) concentrations, with high Th/U ratios of 0.9–4.2 and older $^{206}Pb/^{238}U$ ages ranging from 480 to 452 Ma, inherited from older lithologies during magma ascent. The remaining ten analyses yielded lower U (459–1751 ppm), Th (471–3002 ppm) concentrations, with lower Th/U ratios of 0.8–2.7 with $^{206}Pb/^{238}U$ ages between 440 and 431 Ma, with a weighted mean age of 435.0 ± 4.5 Ma (MSWD = 2.3; Fig. 10A). It is interpreted as the magma crystallization age of the coarse-grained gabbro in this study. Six analyses from the fine-grained gabbro have variable U (985–1652 ppm) and Th (965–2017 ppm) concentrations, with high Th/U ratios of 0.9–1.8. The analyses yielded $^{206}Pb/^{238}U$ ages between 451 and 472 Ma, with a weighted mean age of 461.8 ± 8.2 Ma (MSWD = 3.5; Fig. 10B) and is interpreted as the magma crystallization age of the fine-grained gabbro in this study.

5. Discussion

During the Early Paleozoic, the Alborz and Central Iran blocks were rifted from the northern margin of the Gondwana supercontinent, which was adjacent to what are presently Asiatic Hunic terrains. At $\sim 520\text{--}404$ Ma (Early Cambrian to Early Devonian), igneous activity related to the opening of Paleotethys took place in the NE (Soltan Meidan: Derakhshi et al., 2017), NW (Maku: Valinasab Zarnagh et al., 2021), central (Bafq: Niktabar and Rashidnejad Omran, 2016; Ardakan: Nouri et al., 2022), SE (Zarand: Vesali et al., 2020) and south (salt domes of the high Zagros; Taghipour et al., 2008) of Iran, and record early to late stages of the continental break up that resulted in the opening of the Paleotethys (Moghadam et al., 2015). In this discussion, we consider three aspects of the Early Paleozoic magmatism: (1) petrogenesis of magmatic rocks in the Binaloud zone, (2) implications for Early Paleozoic alkaline

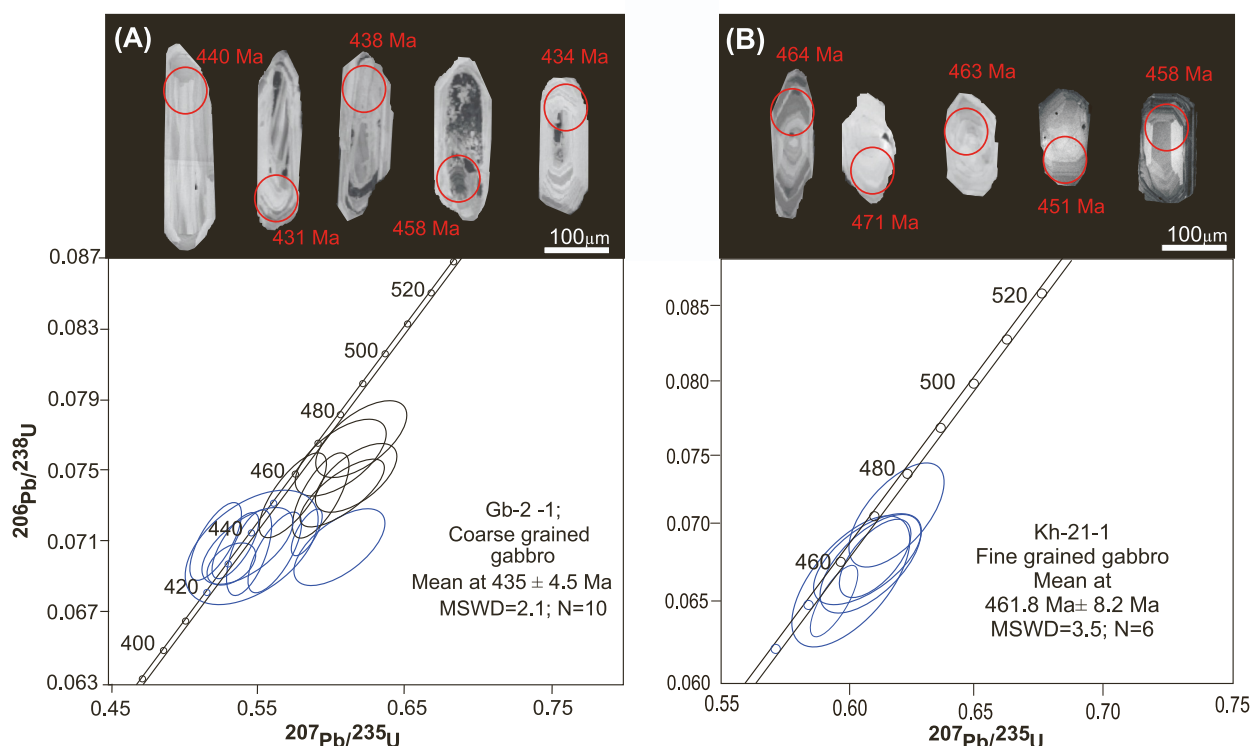


Fig. 10. (A) Cathodoluminescence (CL) images of zircon grains and (B) U–Pb concordia diagrams for the coarse-grained gabbro and corresponding U–Pb ages.

magmatism in Iran, and (3) geodynamic implications for the formation of the Binaloud igneous rocks.

5.1. Petrogenesis of magmatic rocks in the Binaloud zone

The Binaloud magmatic rocks comprise basalt, fine- and coarse-grained gabbro (~461–435 Ma), which have geochemical characteristics resembling alkaline magmatic rocks. The Binaloud alkaline magmatic rocks are characterized by low concentrations of SiO₂ (43.8–52.6 wt%; Supplementary Table S2), indicating that they were derived dominantly from a mantle source. However, the concentrations of MgO (2.1–8.7 wt%), Mg# (14–43), Cr (10–80 ppm), and Ni (11–191 ppm) (Supplementary Table S2) are significantly lower than in primitive basaltic lavas (MgO = 8–11 wt%, Mg# = 63–71, Cr = 266–575 ppm, and Ni = 85–245 ppm) (Kelemen et al., 2007), suggesting that they were formed from melts, which have experienced fractionation of mafic minerals (e.g., olivine and clinopyroxene). The low values of Mg# (40–67) in clinopyroxene from the coarse- and fine-grained gabbro also confirm this explanation. Plagioclase from a coarse-grained gabbro displays a low portion of anorthite (41–64) (Supplementary Table S1b), in particular, in rims (Fig. 6B), suggesting fractional crystallization of plagioclase. Most of the Binaloud basalt and gabbro have low Mg#, identical to other Ordovician-Silurian basalts of the eastern Alborz (e.g., Soltan Meidan; Derakhshi et al., 2017) and southeast of Iran (Jalal Abad; Vesali et al., 2020), as well as low Ni (11–81 ppm) and Cr (6.4–105 ppm) concentrations, suggesting olivine (ol) and clinopyroxene (cpx) fractionational crystallization. Major and trace element data (e.g. CaO/

Al₂O₃ ratios and Al₂O₃, Ni and Cr) vs. MgO also show clear trends against typical indices of fractionation (Supplementary Fig. S1), which is supported by olivine, clinopyroxene and plagioclase phenocrysts being present in the rocks (Fram et al., 1997). Inverse relationships between CaO/Al₂O₃ vs. MgO (Supplementary Fig. S1) indicate a trend towards pyroxene and plagioclase fractionation (Supplementary Fig. S1). However, there is very little variation in Al₂O₃ concentrations between samples, indicating that feldspar fractionation was not important. Because the compositional trends between basalt and gabbro are similar (Supplementary Fig. S1 and Fig. 11), the compositional similarity among these groups can be attributed to the same fractionation process.

The coarse- and fine-grained gabbros from Binaloud have lower MgO, Mg# and SiO₂ than the basalt samples (Supplementary Table S2). Clinopyroxene from both coarse- and fine-grained gabbro also have lower MgO and Mg# than those in the basalt samples (Supplementary Table S1). Thus, it is possible that the coarse- and fine-grained gabbro could be the products directly evolved from the same basaltic melts. This inference is also supported by isotopic evidence, because the Nd isotopic compositions are similar in the gabbro and basalt samples. However, some samples have higher Sr isotopic ratios, which are attributed to interaction with seawater or some other alteration process (Supplementary Table S3; Fig. 9). It is obvious that the coarse- and fine-grained gabbro could have experienced stronger fractional crystallization processes, but the basalt samples may have been sourced by more isotopically depleted components with mixing between mantle and crust derived rocks.

Most studied samples in the Binaloud zone, including alkaline basalt,

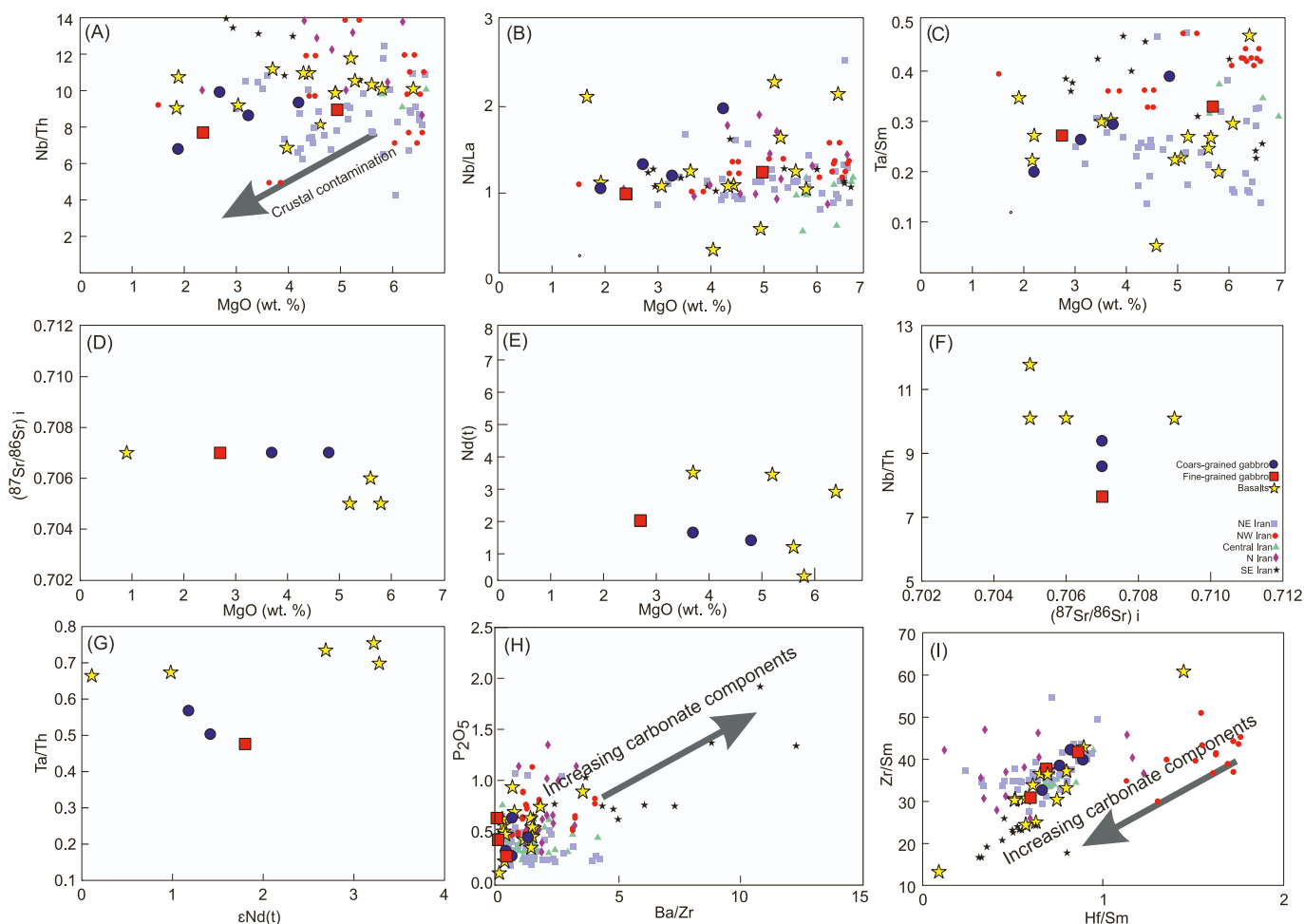


Fig. 11. Plots of (A–E) Nb/Th, Nb/La, Ta/Sm, *ISr* and $\epsilon\text{Nd}(t)$ versus MgO; (F) Nb/Th versus *ISr*; (G) Ta/Th versus $\epsilon\text{Nd}(t)$; (H) P₂O₅ versus Ba/Zr and (I) Zr/Sm versus Hf/Sm Pversus MgO] as in Fig. 6.

fine- and coarse-grained gabbros exhibit OIB-type and E-MORB geochemical features (Fig. 8), in agreement with their pyroxene chemistry (Fig. 6E,F), which are different from arc volcanic rocks, and N-MORB. Such signatures are consistent with plume-related oceanic basalts or continental flood basalts (Hofmann, 1997). Fitton et al. (1997) have proposed the ΔNb approach [$\Delta Nb = 1.74 + \log(Nb/Y) - 1.92 \log(Zr/Y)$] for identifying the mantle source of mafic rocks. Mafic magmas derived from plume-type mantle sources have $\Delta Nb > 0$, whereas magmas derived from depleted mantle and the crust show $\Delta Nb < 0$. Almost all the Binaloud gabbro and basaltic rocks having OIB affinity show positive ΔNb values, indicating a plume geochemical signature. Moreover, when plotted in Fig. 12b, all samples from the Binaloud lie on the line of typical OIB compositions (Sun and McDonough, 1989). Most studied samples in the Binaloud zone, including basalt, fine- and coarse-grained gabbros, exhibit present-day E-MORB and OIB-type geochemical features (Figs. 8 and 12), which are different from arc volcanic rocks, and N-MORB. In the traditional discrimination diagrams, e.g., Ti–V diagram of Shervais (1982), and Zr–Zr/Y diagram of Pearce and Norry (1979), all samples plot in the E-MORB and OIB or within-plate basalt (WPB) fields (Fig. 13A–B). Such signatures are consistent with hot spot or plume-related oceanic island basalts or continental flood basalts (Hofmann, 1997; Condie, 2001). They also show similar Sr and Nd isotopic compositions as those of the oceanic island mantle plume/deep mantle in the word (Zindler and Hart, 1986), Paleozoic OIB-like rocks and some of E-MORB like rocks in the Soltan Meidan basalt sections of the Alborz and Zarand alkaline mafic rocks in SE Iran, as well as central parts of Indo-Australia orogenic belt, central-east Asia (Fig. 9), indicating that their parent magmas were probably derived from a comparably enriched asthenosphere/mantle plume.

The systematic correlations of the elemental and isotopic compositions of the basalt, and coarse- and fine-grained gabbros (Fig. 11) suggest that, in addition to the mantle plume (asthenosphere melts), other reservoirs were also involved in their genesis. A lithospheric mantle and/or a continental crust could be typical contaminants during the evolution of mantle plume/asthenosphere-derived mafic melts (Goring et al., 2003). There is no correlation between Nb/Th and MgO (Fig. 11A) of basaltic samples, combined with the lower MgO concentrations of basaltic samples and lower initial $^{87}\text{Sr}/^{86}\text{Sr}$ ratios (Fig. 11B–C). This agrees with insignificant crustal contamination of a basaltic magma. However, the fine- and coarse-grained gabbro types are characterized by a positive correlation between Nb/Th and MgO (Fig. 11A) and more enriched initial $^{87}\text{Sr}/^{86}\text{Sr}$ ratios and lower $\epsilon\text{Nd}(t)$ values (Fig. 11D–E), which is consistent with a higher contamination of continental crust with respect to basalt samples (Fig. 11A). However, the MgO concentrations of coarse- and fine-grained gabbroic samples are different. They have the same and relatively high initial $^{87}\text{Sr}/^{86}\text{Sr}$ ratios (Fig. 11D), which indicates the same crustal contamination. In addition, the continental crust is characterized by low Nb/U ratios, whereas the Binaloud basalt and gabbro have high Nb/U ratios of 13.3 to 43.5, similar to the range of oceanic island basalts (OIBs) and mid-ocean ridge basalts (MORBs; Hofmann et al., 1986). In addition, because the continental crust is enriched in Ba relative to Nb (Rudnick and Gao, 2014), if crustal contamination had occurred, Ba/Nb ratios should be positively correlated with SiO_2 , which is not observed in our samples (Supplementary Table S2). Therefore, except one sample, we conclude that the crustal contamination was limited during the ascent of the Binaloud mafic magmas, in particular for the basaltic melts.

On the other hand, the enrichment of highly incompatible elements, low Nb/La ratios (< 2.7), high $^{87}\text{Sr}/^{86}\text{Sr}$ ratios (> 0.705), and $\text{K}_2\text{O} + \text{Na}_2\text{O}$ of ~ 5 wt% suggest the involvement of a lithospheric component in the source region (Cousens et al., 2011). A higher Zr/Hf ratio in both basalt and gabbro in our study (39.3–47.3) relative to the OIB value ($\text{Zr}/\text{Hf} = 35.89$; Sun and McDonough, 1989) shows the involvement of lithospheric mantle components. As shown in Figs. 12A–C and 13A–B, there is clear similarity between the basalt and gabbro samples in this

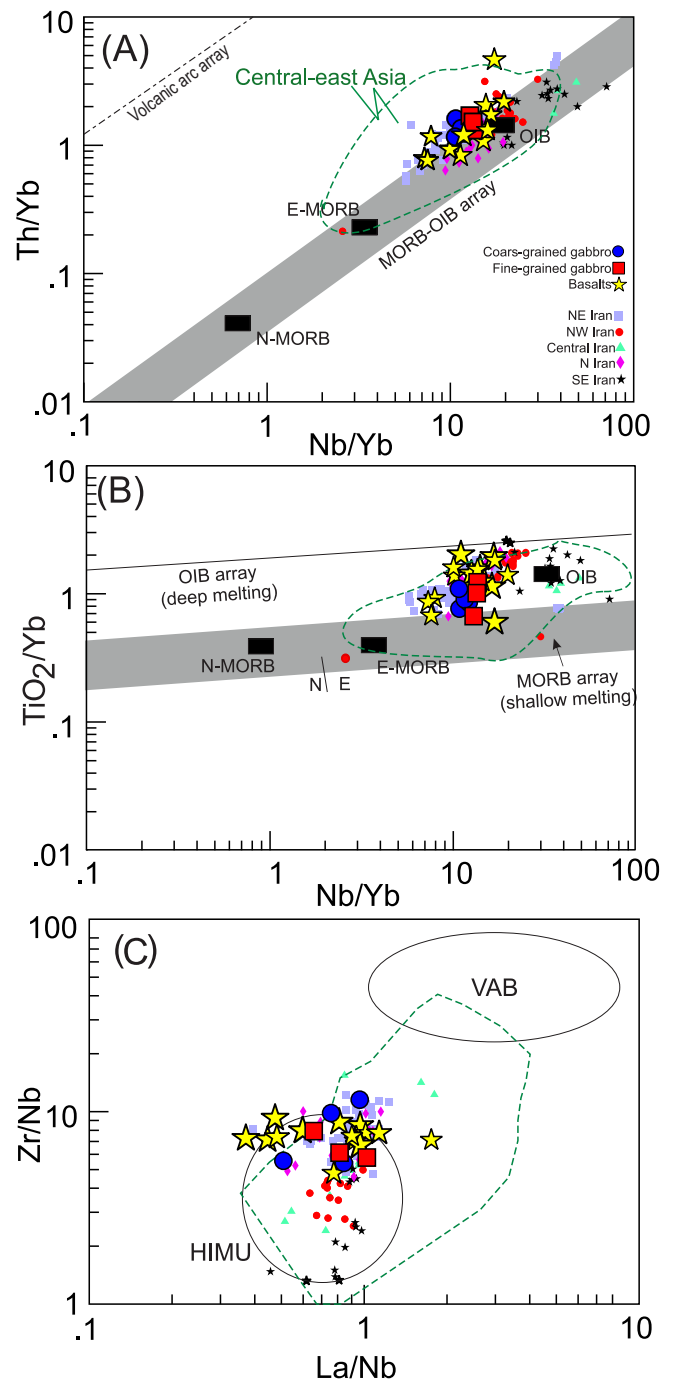


Fig. 12. Discrimination diagrams of (A) Th/Yb versus Nb/Yb (Pearce, 2008), (B) TiO_2/Yb versus Nb/Yb (Macera et al., 2008), (c) Zr/Nb versus La/Nb (Pearce and Norry, 1979).

study with the Early Paleozoic OIB-type and transitional OIB–/back-arc-type basaltic rocks in the northeast, northwest, central and southeast of Iran, which are characterized by interaction of an asthenospheric mantle with a lithospheric melt (Derakhshi et al., 2017; Niktabar and Rashidnejad Omran, 2016; Sacconi et al., 2013; Vesali et al., 2020). Most of the incompatible trace element ratios (Zr/Nb, La/Nb, and Th/La) of the Binaloud mafic rocks (with high MgO > 5 wt%) have remarkable similarities (averages of 8.0, 0.87, and 0.12, respectively) with trace element ratios compatible with an EM1-OIB source (4.2–11.5, 0.86–1.19, and 0.107–0.128, respectively (Saunders et al., 1988; Weaver, 1991). However, their Ba/Nb, Ba/Th and Ba/La ratios are near the EM2-OIB (7.3–13.3, 67–84 and 8.3–11.3, respectively) values with

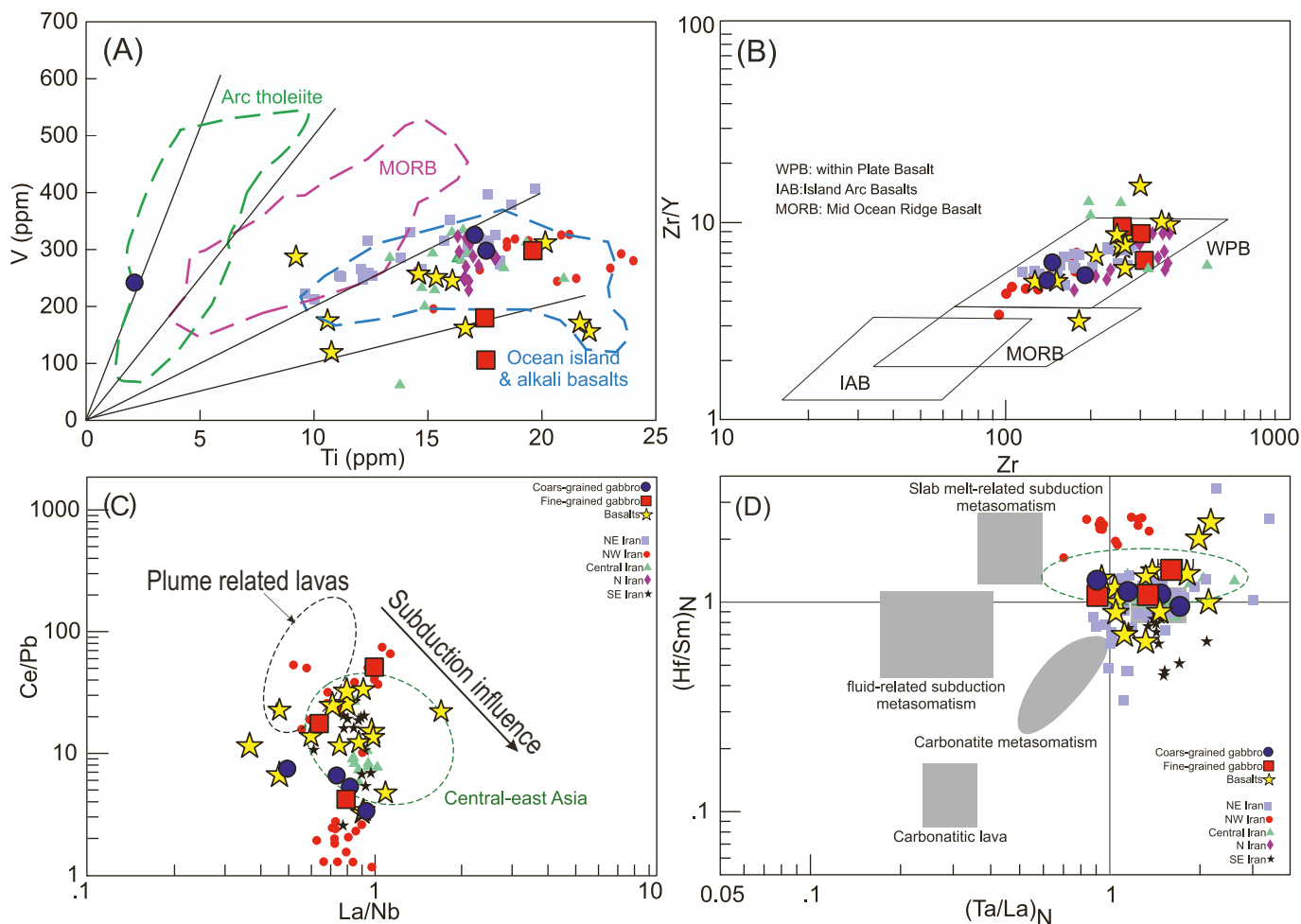


Fig. 13. Discrimination diagrams of (A) Ti vs. V from Shervais (1982); Zr vs. Zr/Y from Pearce and Norry (1979); (C) Ce/Pb versus La/Nb and (D) (Hf/Sm)_N versus (Ta/La)_N (La Fleche et al., 1998) for the fine-, coarse-grained gabbro and basalts in the Binaloud, northeast Iran. Data sources same as in Fig. 6.

average values of 0.8, 83 and 10.1, respectively. In fact, the chemical signatures of the SCLM are imparted into the plume-derived melts through the plume-lithosphere interaction (Song et al., 2008; He et al., 2010). Therefore, we conclude that the Binaloud basalt has been generated by mixing of a subcontinental lithospheric mantle (EM1/EM2 end-member component) with a melt that originated from an asthenospheric mantle plume source.

The REE compositions of mafic rocks are sensitive to the mineralogy

of their magma sources and can be used to constrain the depth of partial melting and melting degrees. As shown in Fig. 14A–B, the basalt and coarse- and fine-grained gabbro samples, with relatively depleted Sr–Nd isotopic compositions (Supplementary Table S3), have not been significantly influenced by later addition of crustal melts during their genesis and could have been generated by low degrees (1–5%) of partial melting of a mantle peridotite in the transitional spinel-garnet stability field (~70–80 km; Gorrington et al., 2003), according to geochemical

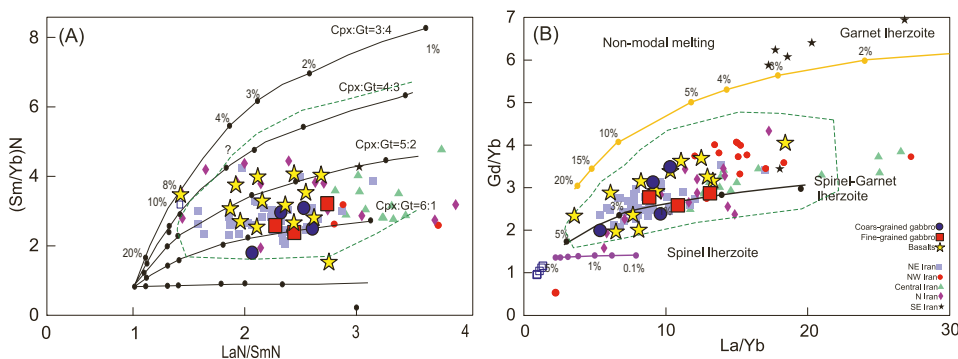


Fig. 14. (A) Sm/Yb versus La/Sm diagram for the basalt and gabbroic rocks in this study. Batch melting trends come from D’Orazio et al. (2001); (B) Gd/Yb versus La/Yb plot. Also shown in (B) are nonmodal batch melting curves calculated for spinel Iherzolite (with mode and melt mode of Ol0:53 + Opx0:27 + Cpx0:17 + Sp0:03 and Ol - 0:06 + Opx0:28 + Cpx0:67 + Sp0:11, respectively) (Kinzler, 1997), spinel-garnet Iherzolite (with mode and melt mode of Ol0:559 + Opx0:25 + Cpx0:14 + Gt0:021 + Sp0:03 and Ol0:05 + Opx0:05 + Cpx0:30 + Gt0:28 + Sp0:32, respectively) (Colakoglu et al., 2012), and garnet Iherzolite (with mode and melt mode of Ol0:60 + Opx0:20 + Cpx0:10 + Gt0:10 and Ol0:03 + Opx - 0:16 + Cpx0:88 + Gt0:09, respectively) (Walter, 1998). Composition of

mantle source was assumed to be the same as those of primitive mantle (Sun and McDonough, 1989). Partition coefficients are from McKenzie and Onions (McKenzie and O’Nions, 1991). The numbers on each curve (or line) correspond to degrees of partial melting.

modelling using batch equilibrium melting and non-modal melting equations. Therefore, we suggest that the Early Paleozoic gabbro and basalt of this study have been derived by partial melting of a spinel-garnet transitional facies asthenospheric mantle at a depth of ~70–80 km, followed by different degrees of fractional crystallization of olivine, clinopyroxene, and plagioclase and mixing with a small component of crustal melts.

5.2. Implications for Early Paleozoic alkaline magmatism in Iran

One of the main queries related to the origin and evolution of the Binaloud magmatic rocks is how they can be related to other magmatic rock exposures of similar age elsewhere in Iran.

Early Paleozoic igneous rocks in Iran are mainly mafic to intermediate in composition with subsidiary felsic intrusive rocks (A-type granites), and are mostly classified as within-plate (WP) magmatic rocks (Moghadam et al., 2015). Ordovician-Silurian alkaline gabbro associated with volcanic rocks are common in NE Iran (e.g. Soltan-Meidan Derakhshi et al., 2017, this study), central-SE Iran (Bafq: Niktabar and Rashidnejad Omran, 2016; Jalal Abad; Vesali et al., 2020) and NW Iran (Misho mafic complex; Saccani et al., 2013). Moghadam et al. (2017) identified Late Cambrian to Early Devonian ages (~492–404 Ma) in detrital zircon of the NE Iran. These authors believe that the age of at 0.5–0.4 Ga records the start of Gondwana rifting and the opening of Paleotethys in Late Cambrian–Ordovician times. Ordovician alkaline gabbro associated with volcanic rocks in the Soltan–Meidan Formation, NE Iran, marks the early stages of rifting and Paleotethys opening (Moghadam et al., 2017). The andesitic and basaltic lavas of the Qelli Formation north of Shirooyeh village, also in the NE Iran, are slightly older than the Soltan–Meidan basalt. It suggests that the Paleozoic rift-related magmatic activities started earlier in northeastern Iran. However, there are no available geochemical data for them.

Moghadam et al. (2017) published Paleozoic ages of detrital zircons, range from 492 Ma to 404 Ma (peak at 450 Ma) in NE Iran for the (i) gabbroic rocks in the Qeli formation, which has a zircon rim U–Pb ages of 463–465 Ma and zircon core ages of 480–470 Ma, and (ii) A-type granitic pebbles within the conglomerate Member 1 of the Padeha Formation with an Early Silurian age of 441 Ma. The zircon eHf(t) values of +8.2 to +2.5 from A-type granitic pebbles within Member 1 of the Padeha Formation reported by these authors is consistent with melts derived from an enriched mantle source. The sandstone and micro-conglomerate of the Ghelli and Padeha formations contain magmatic clasts similar to the gabbro, volcanic rocks and especially A-type granite, showing that such rocks were also exposed to the surface during the Early Paleozoic. Therefore, the youngest age peak of ca 450 Ma, along with the age of A-type granites (441 Ma) indicate that Gondwana rifting and Paleotethys opening probably started in the Late Ordovician. The gabbro samples of this study occur as intrusions, interlayered with mafic volcanic rocks and have a magma crystallization age of 435 ± 4.5 Ma (Fig. 10), indicating that they formed during the Silurian. They are relatively enriched in Nb (25.1–52.7 ppm), Ta (1.5–3.3 ppm), and TiO₂ (2.6–2.8 wt%), and none of them show obvious Nb–Ta depletions (Fig. 8A–D), indicative of their affinity with intraplate extensional basin basaltic rocks (Wilson, 1989). They are LREE-enriched and exhibit OIB-like and transitional OIB/E-MORB-like geochemical characteristics in the Th/Yb vs. Nb/Yb diagram (Fig. 12A), with no clear subduction-related signatures.

The alkaline volcanic rocks in the Soltan–Meidan Formation (Derakhshi et al., 2017) also have enriched isotopic compositions (Fig. 12), as well as low (Ce, Nd, Sr)/Pb ratios, and thus could also show an enriched source for the northeastern Iranian intraplate extensional basin rocks. They display typical incompatible-element characteristics of OIB volcanism, such as no depletion in Nb, Ti and an enrichment in LREE relative to HREE on diagrams with concentrations normalized to primitive mantle (Fig. 7). This feature is common for the OIB melts observed in the Early Paleozoic volcanic provinces of Iran (Fig. 8). The

oldest crustal model ages for the Early Paleozoic intraplate rocks are ~1.5 Ga for NE Iran. Most of the volcanic rocks in the Soltan–Meidan Formation (Derakhshi et al., 2017) and Binaloud (this study) have mafic composition with transitional to alkaline natures (within-plate geochemical signature) and high concentrations of REEs, Nb and Zr, which indicate an origine from the partial melting of a garnet peridotite mantle source within a rift-related tectonic setting (Derakhshi and Ghasemi, 2015).

Saccani et al. (2013) reported new petrological, geochemical and geochronological data from the Misho Mafic Complex (NW Iran) and suggested that mafic–ultramafic rocks represent an Early Carboniferous (356.7 Ma) magmatic event developed during the continental break-up of the northern edge of Gondwana, which led to the opening of Paleotethys. Most of the volcanic rocks in the Misho Mafic Complex (Saccani et al., 2013) have also mafic compositions with an alkaline nature (within-plate geochemical signature). This is consistent with well-documented Late Devonian–Early Carboniferous mantle plume activity to the east, along the Paleotethys margins in central-eastern Asia, and suggests that the initial rift-drift tectonics of the Paleotethys started later in northwestern Iran.

Vesali et al. (2020) reported new petrological, geochemical and geochronological data from the Early Paleozoic Jalal Abad Mafic Complex, SE Iran. Their chondrite-normalized REE and multi-element spider diagrams (Fig. 8), along with high ²⁰⁶Pb/²⁰⁴Pb ratios (18.46–19.83) for the Jalal Abad gabbro, diorite, and diabase dikes, indicate involvement of an OIB-like source during the formation of these rocks. Uranium–lead zircon ages of 425.5 ± 8.6 Ma for mafic rocks of Jalal Abad suggest that the extensional tectonic regime responsible for rifting and opening of the Paleotethys occurred during the Silurian in SE Iran. The oldest Re-depletion ages for SE Iran are ~1.1 Ga (Vesali et al., 2020), which is younger than those from NE Iran.

5.3. Tectonic implications: questions about any relationship with long-lived mantle plume activity

Following the assemblage of the Gondwana supercontinent, which started in the Cryogenian and Ediacaran (Collins and Pisarevsky, 2005), Neoproterozoic–Early Cambrian Cadomian arc-type magmatism occurred for several thousand kilometers along the Cadomian–Avalonian orogenic belt (Linnemann et al., 2014; Pereira et al., 2011; Ustaömer et al., 2009). It is proposed that Gondwanan terranes along the Cadomian–Avalonian orogenic belt might have formed as back-arc basins, where sediments of Cadomian age were deposited (Nance and Murphy, 1994). In Late Cambrian–Early Ordovician time (ca 490–480 Ma), after uplift, rifting and magmatism in northern Gondwana, opening of the Paleotethys started (Fig. 15). Further to the northeast, the Tarim, Afghanistan and Lhasa blocks were detached. A juvenile rift-related magmatism, related to the breakup of a supercontinent and opening of an oceanic basin also took place in Iran (basalts, A-type granites and alkaline gabbros), which were the main sources of the ~0.4 Ga detrital zircons in the sedimentary rocks (Moghadam et al., 2016). This raises the question about the major cause of the supercontinent breakup and the opening of an oceanic basin during Ordovician–Silurian, and if they were related to a back-arc.

Nance et al. (2010) concluded that arc and back-arc basin activity led to the Early Paleozoic rifting of Gondwana at ~530 to 485 Ma, to open the Rheic Ocean. The Late Cambrian to Early Ordovician separation of the Avalonian terranes opened the Rheic Ocean, which expanded at a fast rate, a process linked to slab pull. This activity was simultaneous with, and presumably related to subduction of the Iapetus oceanic crust at the Laurentian margin, where it resulted in the extensive development of ophiolite and arc sequences, associated with accretionary tectonics (e.g. van Staal and Barr, 2012). The mechanisms responsible for the Early Paleozoic extensional processes of the Cadomian terranes are not always evident. Neubauer (2002) suggests development of back-arcs and subsequent separations, based mainly on a consideration of Cambrian

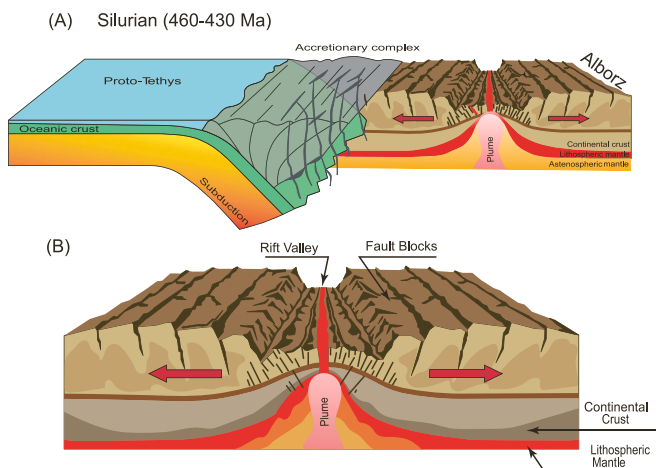


Fig. 15. (A) Schematic model showing previous subduction of Protpetthys and stretching force for breakup of a continent and opening of the oceanic plate; (B) Early Paleozoic rifting and the opening of Paleo-Tethys in the northeast Iran in closed view. Details are discussed in the text.

activity in the Cadomian terranes. However, the within plate OIB-like features of associated Silurian magmatic rocks differ from those of Early Paleozoic calc-alkaline rocks formed in the back-arc basin, suggesting plume source activity for their generation (Fig. 12). In addition, several studies show that the calc-alkaline-shoshonitic and alkaline suites formed simultaneously in a back-arc setting (Sepidbar et al., 2020; Moghadam et al., 2018), which is not the case of alkaline Early Paleozoic rocks of Iran. Extensional rifts related to back-arc can be related to slab roll-back, which can also be responsible for coeval arc magmatic flare-ups and exhumation of subduction-related high-pressure rocks (Ducea et al., 2017). This is also not the case of our study. Extension and crustal thinning related to back-arc permit decompression melting of the subcontinental lithospheric mantle (=SCLM) or sub-arc mantle beneath the retro-arc (Sepidbar et al., 2020). Low degree of melting of an enriched SCLM and/or plume-influenced sub-arc mantle can generate OIB-like melts. Such melts may differ from OIB-like melts from oceanic islands and/or continental plumes, which are isotopically more evolved, similarly to the isotopic signatures of our study, suggesting plume mantle activity. Mantle plumes also affect a larger area, with a diameter of >300 km (e.g., Poore et al., 2011), which is the case for Iran's Ordovician-Silurian exposures, including the ones of this study. The following lines of evidence also give convincing support for their mantle plume origin of alkaline mafic rocks: (i) The exposures related to plume mantle activity and Paleotethys opening contain abundant alkali continental basalt (Soltan–Meidan basalt), felsic–mafic plutons (with ages of ca. 490–405 Ma; Moghadam et al., 2017) and dolomite, evaporitic and terrigenous sedimentary rocks in the Ordovician Ghelli and early Devonian Padeha formations in the Alborz (Stampfli, 1978). (ii) The mafic rocks in accretionary wedges are regarded as plume-related oceanic-island fragments (Safonova et al., 2016; Yang et al., 2015). Therefore, they can coexist with oceanic fragments and deep marine or slope facies sedimentary rocks, such as carbonate, chert, and volcanic clastic rocks. The volcanic and gabbroic rocks in the the Binaloud zone coexist with deep marine or slope facies sedimentary rocks, such as carbonate and volcanic clastic rocks, which are not associated with ophiolite, and which confirms their formation in a plume-related oceanic setting. (iii) Ridge subduction is common in modern and ancient accretionary orogenic belts (Sisson et al., 2003). Such ridge subduction processes can result in the opening of a slab window and generation of intense magmatism and metamorphism in a near-trench position, with the formation of adakite, high-Mg andesitic rocks, tholeiitic and alkaline basalt, high-Ca boninite, and A-type granite, and associated low-pressure/high-temperature metamorphic rocks.

However, except for the alkaline basalt, gabbro and A-type granite (Moghadam et al., 2016), most of the magmatic and metamorphic products mentioned above are lacking in our study area (Fig. 4). Therefore, the basalt and gabbro of our study area are probably not related to any ridge subduction-related setting. (iv) The plume-related continental rifts are commonly generated during break-up of supercontinents, and are formed before the opening of the oceanic basin (Fan et al., 2013). Mantle plume activity leads to formation of Fe–Ti rich magmas (Khedr et al., 2020, 2022).

The basaltic and gabbroic rocks in our study area are enriched in iron oxides (up to 10 vol%) and occur near a suture zone, and their formation was coeval or slightly older than the initial opening time of the Paleotethys rift. Thus, their generation could be associated with the plume-related continental rifting.

Several studies propose that mantle plumes play main roles in continent separation, and they may be active for a long time before the break-up of continents and the formation of oceans. For example, the activity of the mantle plume within the Rodinia supercontinent started at ca. 850 Ma and lasted to ca. 750 Ma (Song et al., 2010), but the birth of oceans took place after 600 Ma (Zhao et al., 2018). A more recent example is the East African Rift system, where there has been slow extension since the plume impact at ca. 45 Ma, but without continental break-up to date (Rogers et al., 2000). The basalt and gabbro of this study, which have OIB-like or transitional OIB/E-MORB-like geochemical characteristics, have yielded a Silurian age (435 Ma). As shown in the Supplementary Table S4, all zircon ages indicate three major peaks at 460 Ma, 440 Ma, and 430 Ma (Mean ages at 435 Ma), suggesting a multi-staged, intermittent magmatic activity. The 461.8 Ma ages of fine-grained gabbro along with old ages of zircons (460–440 Ma) from coarse-grained gabbroic rocks may represent the initial magmas along fractures during plume upwelling, while the large-scale eruption of the mantle plume may have occurred at ca. 435 Ma. The older ages of mafic rocks are also reported by Derakhshi et al. (2022) for coarse-grained gabbro from Buzhan area in the Binaloud zone, suggesting that mantle plume activity in the Binaloud zone to be as old as 460 Ma and lasted to ca. 435 Ma, for 25 m.y. These ages are older or similar with respect to the opening of the Paleo-Tethys Ocean. These ages are also significantly younger than the timing of the back-arc opening in NE Iran, and thus can reveal and confirm the timing of the plume magmatic activity of the Binaloud gabbro-basalt complex. Therefore, as a consequence, we suggest that continental lithosphere was firstly weakened by previous subduction-induced mantle flow activity (Fig. 15) during the Cadomian. The stretching for break-up of a continent and opening of the oceanic plate was provided by long lasting mantle plume activity from 460 to 435 Ma, resulting in the formation of the Binaloud gabbro and basalt in the passive margin.

6. Conclusions

- (1) Basalt and gabbro, located in the northeast of Iran, were emplaced during the Silurian (~461 to 435 Ma). They have OIB-like and transitional OIB–/E-MORB-like geochemical characteristics with an intraplate extensional basin affinity.
- (2) Elemental, isotopic, and mineral chemistry data indicate that they were derived by partial melting of a plume/asthenospheric mantle in the transitional spinel-garnet stability field, followed by interaction with a lithospheric mantle, different degrees of fractional crystallization of olivine, clinopyroxene, and plagioclase and mixing with minor crustal melts.
- (3) Combined with the available data, we suggest that the mantle plume interacted with the continental lithosphere and drove continental break-up and the opening of the Paleo-Tethys Ocean. This took place as a consequence of the previously induced stress generated by roll-back of the subducting Iapetus oceanic plate.

Supplementary data to this article can be found online at <https://doi.org/10.1016/j.lithos.2023.107191>.

org/10.1016/j.lithos.2023.107191.

Declaration of Competing Interest

We declare that we have no known competing financial interests or personal relationships that could have appeared to influence the work reported in this paper.

Acknowledgements

This is a postdoctoral research contribution #3471 funded by Ferdowsi University of Mashhad, Iran. We thank Prof. Greg Shellnutt for editorial handling and Prof. Mohamed Zaki Khedr and one anonymous reviewer for their positive comments and suggestions, allowing us to greatly improve the manuscript. The senior author F. Sepidbar acknowledges support from Ferdowsi University of Mashhad for assistance during field work.

References

- Aharipour, R., Moussavi, M.R., Mosaddegh, H., Mistiaen, B., 2009. Facies features and paleoenvironmental reconstruction of the early to Middle Devonian syn-rift volcano-sedimentary succession (Padeha Formation) in the Eastern-Alborz Mountains, NE Iran. *Facies* 56 (2), 279–294. <https://doi.org/10.1007/s10347-009-0200-x>.
- Alavi-Naini, M., 1972. Etude géologique de la région de Djam. Geological Survey of Iran. Reports 23, 1–288.
- Arenas, R., Martínez Catalán, J.R., Sánchez Martínez, S., Fernández-Suárez, J., Andonaegui, P., Pearce, J.A., Corfú, F., 2007. The Vila de Cruces Ophiolite: a remnant of the early Rheic Ocean in the Variscan suture of Galicia (Northwest Iberian Massif). *J. Geol.* 115, 129–148.
- Ashouri, A.R., 2002. Palaeogeography (Conodonts; Late Devonian) from the Tabas Region, Eastern Iran. *Iranian Int. J. Sci.* 3 (2), 187–220.
- Ayati, F., Noghreyan, M., Khalili, M., 2011. A review of Palaeozoic magmatism in central Iran. *J. Crystallogr. Mineral.* Iran 18, 615–632.
- Berberian, M., King, G.C.P., 1981. Towards a paleogeography and tectonic evolution of Iran. *Can. J. Earth Sci.* 18, 210–265.
- Bradshaw, J.D., 1989. Cretaceous geotectonic patterns in the New Zealand region. *Tectonics* 8, 803–820.
- Cawood, P.A., Martin, E.L., Murphy, J.B., Pisarevsky, S.A., 2021. Gondwana's interlinked peripheral orogens. *Gondwana's interlinked peripheral orogens. Earth Planet. Sci. Lett.* 568, 117057.
- Colakoglu, K., Sayit, K., Gunay, Goncuoglu, M.C., 2012. Geochemistry of mafic dykes from the southeast A. R. Anatolian ophiolites, Turkey: implications for an intra-oceanic arc basin system. *Lithos* 132–133, 113–126.
- Collins, A.S., Pisarevsky, S.A., 2005. Amalgamating eastern Gondwana: The evolution of the Circum-Indian Orogens. *Earth-Science Reviews* 71 (3–4), 229–270. <https://doi.org/10.1016/j.earscirev.2005>.
- Condie, K.C., 2016. Tectonic settings. In: Condie, K.C. (Ed.), *Earth as an Evolving Planetary System*, third edition. Academic Press, Cambridge, MA, pp. 43–88.
- Cousens, B.L., Henry, C.D., Harvey, B.J., Brownrigg, T., Prytulak, J., Allan, J.F., 2011. Secular variations in magmatism during a continental arc to post-arc transition: Plio-Pleistocene volcanism in the Lake Tahoe/Truckee area, Northern Sierra Nevada, California. *Lithos* 123, 225–242.
- Derakhsh, M., Ghasemi, H., 2015. Soltan Maidan Complex (SMC) in the eastern Alborz structural zone, northern Iran: magmatic evidence for Paleotethys development. *Arab. J. Geosci.* 8, 849–866.
- Derakhsh, M., Ghasemi, H., Miao, L., 2017. Geochemistry and petrogenesis of Soltan Maidan basalts (E Alborz, Iran): implications for asthenosphere-lithosphere interaction and drifting along the N margin of Gondwana. *Chem. Erde* 77, 131–145.
- Derakhsh, M., Ernst, R.E., Kamod, S.R., 2022. Ordovician-Silurian volcanism in northern Iran: implications for a new Large Igneous Province (LIP) and a robust candidate for the Late Ordovician mass extinction. *Gondwana Res.* 107, 256–280.
- Díez Fernández, R., Castiñeiras, P., Gómez Barreiro, J., 2012. Age constraints on Lower Paleozoic convection system: magmatic events in the NW Iberian Gondwana margin. *Gondwana Res.* 21, 1066–1079.
- D'Orazio, M., Agostini, S., Innocenti, F., Haller, M.J., Manetti, P., Mazzarini, F., 2001. Slab window-related magmatism from southernmost South America: the Late Miocene mafic volcanics from the estancia Glencross area (~ 52 S, Argentina–Chile). *Lithos* 57 (2–3), 67–89.
- Ducea, M.N., Bergantz, G.W., Crowley, J.L., Otamendi, J., 2017. Ultrafast magmatic buildup and diversification to produce continental crust during subduction. *Geology* 45, 235–238.
- Fan, H.P., Zhu, W.G., Li, Z.X., et al., 2013. Ca. 1.5 Ga mafic magmatism in South China during the break-up of the supercontinent Nuna/Columbia: the Zhuqing Fe-Ti-V oxide ore-bearing mafic intrusions in western Yangtze block. *Lithos* 168–169, 85–98.
- Fitton, J.G., Saunders, A.D., Norry, M.J., Hardarson, B.S., Taylor, R.N., 1997. *Thermal and chemical structure of the Iceland plume*. *Earth Planet. Sci. Lett.* 153 (3–4), 197–208. [https://doi.org/10.1016/S0012-821X\(97\)00170-2](https://doi.org/10.1016/S0012-821X(97)00170-2).
- Floyd, P.A., Winchester, J.A., Seston, R., Kryza, R., Crowley, Q.G., 2000. Review of geochemical variation in Lower Palaeozoic metabasites from the NE Bohemian Massif: Intracratonic rifting and plume–ridge interaction. In: Franke, W., Haak, V., Oncken, O., Tanner, D. (Eds.), *Orogenic Processes: Quantification and Modelling in the Variscan Belt*. Geological Society, vol. 179. Special Publications, London, pp. 155–174.
- Fram, M. S., Leshner, C. E. & Volpe, A. M., 1997. Mantle melting mantle plume. In: Storey, B. C., Alabaster, T. & Pankhurst, R. J., systematics: the transition. *J. Petrol.*, 38 (2) 231–275.
- Ghasemi, H., Derakhsh, M., 2008. Mineralogy, geochemistry, and role of olivine mechanical separation in the generation of Lower Paleozoic igneous rocks in Shirgasht area, NW of Tabas, Central Iran. *Iranian J. Crystallogr. Mineral.* 16 (2), 207–224.
- Ghavidel-Syook, M., 2008. Palynostratigraphy and Palaeogeography of the Upper Ordovician Gorgan Schists (Southeastern Caspian Sea), Eastern Alborz Mountain Ranges, Northern Iran. *Comunicações Geológicas* 95, 123–155.
- Ghavidel-Syooki, G., Hassanzadeh, J., Vecoli, M., 2011. Palynology and isotope geochronology of the Upper Ordovician-Silurian successions (Ghelli and Soltan Maidan Formations) in the Khoshyeilagh area, eastern Alborz Range, northern Iran; stratigraphic and palaeogeographic implications. *Rev. Palaeobot. Palynol.* 164, 251–271.
- Gorring, M., Singer, B., Gowers, J., Kay, S.M., 2003. Plio-Pleistocene basalts from the Meseta del Lago Buenos Aires, Argentina: evidence for asthenosphere-lithosphere interactions during slab window magmatism. *Chem. Geol.* 193 (3–4), 215–235.
- He, Q., Xiao, L., Balta, B., Gao, R., Chen, J., 2010. Variety and complexity of the Late-Permian Emeishan basalts: Reappraisal of plume-lithosphere interaction process. *Lithos* 119, 91–107.
- Hofmann, D.A., 1997. An overview of the logic and rationale of hierarchical linear models. *Journal of Management* 23 (6), 723–744.
- Hofmann, A.W., Jochum, K.P., Seufert, M., White, W.M., 1986. Nb and Pb in oceanic basalts: new constraints on mantle evolution. *Earth Planet. Sci. Lett.* 79, 33–45.
- Honarmand, M., Xiao, W.J., Nabatian, G., Blades, M.L., dos Santos, M.C., Collins, A.S., Ao, S.J., 2018. Zircon U-Pb-Hf isotopes, bulk-rock geochemistry and Sr-Nd-Pb isotopes from late Neoproterozoic basement in the Mahneshan area, NW Iran: implications for Ediacaran active continental margin along the northern Gondwana and constraints on the late Oligocene crustal anatexis. *Gondwana Res.* 57, 48–76.
- Hushmandzadeh, A., Alavi-Naini, M., Haghighipour, A., 1978. Geological Evolution of Torud Area (Precambrian to Recent). Geological Survey of Iran (in Persian), Tehran, Iran.
- Jamshidipour, A., 2022. Evaluation of geotourism for Gonabad Qasabeh Qanat: Potentials and capabilities. *Geoconserv. Res.* 5 (2), 347–356. <https://doi.org/10.30486/gcr.2023.1975865.1119>.
- Kelemen, P.B., Hanghøj, K., Greene, A.R., 2007. One view of the geochemistry of subduction-related magmatic arcs, with an emphasis on primitive andesite and lower crust: treatise on. *Geochemistry* 3, 593–659.
- Khedr, M.Z., El-Awady, A., Arai, S., Hauzenberger, C., Tamura, A., Stern, R.J., Morishita, T., 2020. Petrogenesis of the ~740 Korab Kansi mafic-ultramafic intrusion, South Eastern Desert of Egypt: evidence of Ti-rich ferropicritic magmatism. *Gondwana Res.* 82, 48–72.
- Khedr, M.Z., Takazawa, E., Arai, S., Stern, R.J., Morishita, T., El-Awady, A., 2022. Styles of Fe-Ti-V ore deposits in the Neoproterozoic layered mafic-ultramafic intrusions, south Eastern Desert of Egypt: evidence for fractional crystallization of V-rich melts. *J. Afr. Earth Sci.* 194, 104620.
- Kinzler, R.J., 1997. Melting of mantle peridotite at pressures approaching the spinel to garnet transition: application to mid-ocean ridge basalt petrogenesis. *J. Geophys. Res.-Solid Earth* 102, 853–874.
- La Fleche, M.R., Camire, G., Jenner, G.A., 1998. Geochemistry of post-Acadian, Carboniferous continental intraplate basalts from the Maritimes basin, Magdalen islands, Québec, Canada. *Chem. Geol.* 148 (3–4), 115–136.
- Li, T., T. Hasegawa, X. Yin, Y. Zhu, K. Boote, M. Adam, S. Bregaglio, S. Buis, R. Confalonieri, T. Fumoto, D. Gaydon, M. Marcaida, III, H. Nakagawa, P. Oriol, A.C. Ruane, F. Ruget, B. Singh, U. Singh, L. Tang, F. Tao, P. Wilkens, H. Yoshida, Z. Zhang, and B. Bouman, 2015. Uncertainties in predicting rice yield by current crop models under a wide range of climatic conditions. *Glob. Change Biol.*, 21, no. 3, 1328–1341, doi:10.1111/gcb.12758.
- Lin, K.Z., Fraser, I.A., 2003. The use of analytical procedures by external auditors in Canada. *J. Int. Account. Audit. Tax.* 12 (2), 153–168. <https://doi.org/10.1016/j.intaccudtax.2003.08.002>.
- Linnemann, U., Gerdes, A., Hofmann, M., Marko, L., 2014. The Cadomian Orogen: Neoproterozoic to Early Cambrian crustal growth and orogenic zoning along the periphery of the West African Craton—Constraints from U-Pb zircon ages and Hf isotopes (Schwarzburg Antiform, Germany). *Precambrian Res.* 244, 236–278.
- Liu, Y.S., Zong, K.Q., Kelemen, P.B., Gao, S., 2008. Geochemistry and magmatic history of eclogites and ultramafic rocks from the Chinese continental scientific drill hole: subduction and ultrahigh-pressure metamorphism of lower crustal cumulates. *Chem. Geol.* 247, 133–153.
- Ludwig, K.R., 2003. User's manual for Isoplot/Ex version 3.00, a geochronological toolkit for Microsoft Excel. Berkeley Geochronology Center Special Publications 4, 72pp.
- Macara, P., Gasperini, D., Ranalli, G., Mahatsente, R., 2008. Slab detachment and mantle plume upwelling in subduction zones: an example from the Italian South-Eastern Alps. *J. Geodyn.* 45, 32–48.
- McKenzie, D., O'Nions, R.K., 1991. Partial melt distributions from inversion of rare earth element concentrations. *J. Petrol.* 32 (5), 1021–1091.
- Mehdizadeh Shahri, M., 2008. Pre-rifting Evidence of Paleotethys in the Southwest of Shahrood, Northeastern Iran. *World Appl. Sci. J.* 3 (1), 154–161.
- Metcalfe, I., 2021. Multiple Tethyan Ocean basins and orogenic belts in Asia. *Gondwana Res.* 100, 87–130. <https://doi.org/10.1016/j.jgr.2021.01.012>.

- Miskovic, A., Schaltegger, U., 2009. Crustal growth along a non-collisional cratonic margin: a Lu-Hf isotopic survey of the Eastern Cordilleran granitoids of Peru. *Earth Planet. Sci. Lett.* 279, 303–315.
- Moghadam, H.S., Li, X.-H., Ling, X.-X., Stern, R.J., Khedr, M.Z., Chiaradia, M., Ghorbani, G., Arai, S., Tamura, A., 2015. Devonian to Permian evolution of the Paleoe-Tethys Ocean: New evidence from U–Pb zircon dating and Sr–Nd–Pb isotopes of the Darrehanjir–Mashhad “ophiolites”, NE Iran. *Gondw. Res.* 28, 781–799.
- Moghadam, H.S., Li, X.H., Stern, R.J., Santos, J.F., Ghorbani, G., Pourmohsen, M., 2016. Age and nature of 560–520 Ma calc-alkaline granitoids of Biarjmand, Northeast Iran. *Int. Geol. Rev.* 58 (12), 1492–1509.
- Moghadam, H., Li, X.H., Griffin, W.L., Stern, R.J., Thomsen, T.B., Meinhold, G., Aharipour, R., O'Reilly, S.Y., 2017. Early Paleozoic tectonic reconstruction of Iran: tales from detrital zircon geochronology. *Lithos* 268–271, 87–101.
- Moghadam, H.S., Griffin, W.L., Kirchenbauer, M., Garbe-Schönberg, D., Khedr, M.Z., Kimura, J.-I., Stern, R.J., Ghorbani, G., Murphy, R., O'Reilly, S.Y., Arai, S., 2018. Roll-back, Extension and Mantle Upwelling in NW Iran. *J. Petrol.* 59, 1417–1465.
- Nance, R.D., Murphy, J.B., 1994. Contrasting basement isotopic signatures and the palinspastic restoration of peripheral orogens – example from the neoproterozoic Avalonian-Cadomian belt. *Geology* 22, 617–620.
- Muttoni, M., Mattei, M., Balini, A., Zanchi, M., Gaetani, M., Berra, F., 2009. In: Brunet, M., Wilmsen, Granath (Eds.), *South Caspian to Central Iran basins*, 312. Geological Society London Special Publication, pp. 7–29.
- Nance, R.D., Gutierrez-Alonso, G., Keppie, J.D., Linnemann, U., Murphy, J.B., Quesada, C., Strachan, R.A., Woodcock, N.H., 2010. Evolution of the Rheic Ocean. *Gondwana Res.* 17, 194–222.
- Nance, R.D., Gutiérrez-Alonso, G., Keppie, J.D., Linnemann, U., Murphy, J.B., Quesada, C., Strachan, R.A., Woodcock, N.H., 2012. A brief history of the Rheic Ocean. *Geosci. Front.* 3, 125–135.
- Neubauer, F., 2002. Evolution of late Neoproterozoic to early Paleozoic tectonic elements in Central and Southeast European Alpine mountain belts: review and synthesis. *Tectonophysics* 352 (1–2), 87–103. [https://doi.org/10.1016/S0040-1951\(02\)00190-7](https://doi.org/10.1016/S0040-1951(02)00190-7).
- Niktabar, M., Rashidnejad Omran, N., 2016. Geochemistry and petrography of mafic sills within Rizu formation, North of Bafq, Central Iran. *Geochemistry* 5 (3), 261–267.
- Nouri, F., Davoudian, A.R., Shabani, N., Allen, M.B., Asahara, Y., Azizi, H., Anma, R., Khodami, M., Tsuboi, M., 2022. Tectonic transition from Ediacaran continental arc to early Cambrian rift in the NE Ardakan region, central Iran: constraints from geochronology and geochemistry of magmatic rocks. *J. Asian Earth Sci.* 224, 105011.
- Pearce, J.A., 2008. Geochemical fingerprinting of oceanic basalts with applications to ophiolite classification and the search for Archean oceanic crust. *Lithos* 100 (1–4), 14–48.
- Pearce, J.A., Norry, M.J., 1979. Petrogenetic implications of Ti, Zr, Y, and Nb variations in volcanic-rocks. *Contrib. Mineral. Petrol.* 69 (1), 33–47.
- Pereira, M.F., Chichorro, M., Sola, A.R., Silva, J.B., Sanchez-Garcia, T., Bellido, F., 2011. Tracing the Cadomian magmatism with detrital/inherit zircon ages by in-situ U-Pb SHRIMP geochronology (Ossa-Morena Zone, SW Iberian Massif). *Lithos* 123, 204–217.
- Planck, S., Symonds, P.A., Alvestad, E., Skogseid, J., 2000. Seismic volcanostratigraphy of large-volume basaltic extrusive complexes on rifted margins. *J. Geophys. Res.* 105, 19335–19351. <https://doi.org/10.1029/1999JB900005>.
- Poore, H., White, N., MacLennan, J., 2011. Ocean circulation and mantle melting controlled by radial flow of hot pulses in the Iceland plume. *Nature Geosci.* 4 (8), 558–561. <https://doi.org/10.1038/ngeo1161>.
- Ramezani, J., Tucker, R.D., 2003. The Saghand Region, Central Iran: U-Pb geochronology, petrogenesis and implications for Gondwana Tectonics. *Am. J. Sci.* 303, 622–665.
- Richards, M.A., Duncan, R.A., Courtillot, V.E., 1989. Flood basalts and hot-spot tracks: plume heads and tails. *Science* 246, 103–107.
- Rock, N.M.S., 1990. The international mineralogical association (IMA/CNMN) pyroxene nomenclature scheme computerization and its consequences. *Mineral. Petrol.* 43 (2), 99–119.
- Rogers, N., Macdonald, R., Fitton, J.G., George, R., Smith, M., Barreiro, B., 2000. Two mantle plumes beneath the East African rift system: Sr, Nd and Pb isotope evidence from Kenya Rift basalts. *Earth Planet. Sci. Lett.* 176 (3), 387–400. [https://doi.org/10.1016/S0012-821X\(00\)00012-1](https://doi.org/10.1016/S0012-821X(00)00012-1).
- Rubatto, D., Gebauer, D., 2000. Use of cathodoluminescence for U-Pb Zircon dating by ion microprobe: some examples from the western alps. In: Pagel, M., Barbin, V., Blanc, P., Ohnenstetter, D. (Eds.), *Cathodoluminescence in Geosciences*. Springer, Berlin, Heidelberg. https://doi.org/10.1007/978-3-662-04086-7_15.
- Rudnick, R.L., Gao, S., 2014. *Composition of the Continental Crust*. Treatise on Geochemistry 1–51. <https://doi.org/10.1016/B978-0-08-095975-7.00301-6>.
- Saccani, E., Allahyari, Kh., Beccaluva, L., Bianchini, G., 2013. Geochemistry and petrology of the Kermanshah ophiolites (Iran): Implication for the interaction between passive rifting, oceanic accretion, and OIB-type components in the Southern Neo-Tethys Ocean. *Gondw. Res.* 24, 392–411.
- Saccani, E., Azimzadeh, Z., Dilek, Y., Jahangiri, A., 2013. Geochronology and petrology of the Early Carboniferous Misho Mafic Complex (NW Iran), and implications for the melt evolution of Paleo-Tethyan rifting in Western Cimmeria. *Lithos* 162, 264–278.
- Safonova, I., Biske, G., Romer, R.L., Seltmann, R., Simonov, V., Maruyama, S., 2016. Middle Paleozoic mafic magmatism and ocean plate stratigraphy of the South Tianshan, Kyrgyzstan. *Gondwana Res.* 30, 236–256.
- Saunders, A.D., Norry, M.J., Tarney, J., 1988. Origin of MORB and chemically depleted mantle reservoirs: trace element constraints. *J. Petrol.* 415–445.
- Sepidbar, F., Moghadam, H.S., Li, C., Stern, R.J., Jiantang, P., Vesali, Y., 2020. Cadomian Magmatic Rocks from Zarand (SE Iran) Formed in a Retro-Arc Basin. *Lithos* 366–367, 105569.
- Shervais, J.W., 1982. Ti-V plots and the petrogenesis of modern and ophiolitic lavas. *Earth Planet. Sci. Lett.* 59 (1), 101–118. [https://doi.org/10.1016/0012-821X\(82\)90120-0](https://doi.org/10.1016/0012-821X(82)90120-0).
- Sisson, V.B., Pavlis, T.L., Roeske, S.M., Thorkelson, D.J., 2003. Introduction: An overview of ridge-trench interactions in modern and ancient settings. In: Sisson, V.B., Roeske, S.M., Pavlis, T.L. (Eds.), *Geology of a Transpressional Orogen Developed during Ridge-Trench Interaction along the North Pacific Margin*. Boulder, Colorado, Geological Society of America Special Paper, vol. 371, pp. 1–18.
- Smith, J.V., Brown, W.L., 1988. Nomenclature, general properties of feldspars and simple determinative diagrams. In: *Feldspar Minerals*. Springer, Berlin, Heidelberg. https://doi.org/10.1007/978-3-642-72594-4_9.
- Song, X.Y., Qi, H.W., Robinson, P.T., Zhou, M.F., Cao, Z.M., Chen, L.M., 2008. Melting of the subcontinental lithospheric mantle by the Emeishan mantle plume: evidence from the basal alkaline basalts in Dongchuan, Yunnan, Southwestern China. *Lithos* 100, 93–111.
- Song, S.G., Su, L., Li, X.H., Zhang, G.B., Niu, Y.L., Zhang, L.F., 2010. Tracing the 850-Ma continental flood basalts from a piece of subducted continental crust in the North Qaidam UHPM belt, NW China. *Precambrian Res.* 183 (4), 805–816. <https://doi.org/10.1016/j.precamres.2010.09.008>.
- Stampfli, G.M., 1978. Etude géologique générale de l'Elbourz oriental au sud de Gonbad-e-Qabus (Iran NE). PhD thesis. Université de Genève, 329 p.
- Stöcklin, J., 1968. Structural history and tectonics of Iran: a review. *Am. Assoc. Pet. Geol. Bull.* 52, 1229–1258.
- Sun, S.S., McDonough, W.F., 1989. Chemical and isotopic systematics of oceanic basalts: implications for mantle composition and processes. In: Saunders, A.D., Norry, M.J. (Eds.), *Magmatism in the Ocean Basins*, *Geol. Soc. Spec. Publ.* 42, pp. 313–345.
- Taghipour, S., Khalili, M., Noghrehan, M., Toraby, Gh., Mackizadeh, M.A., Taghipour, B., 2008. Mineralogy and petrology in magmatic rocks of Hormoz Formation (salt diapires of High Zagros). *Iran. J. Crystallogr. Mineral.* 16, 3.
- Topuz, G., Hegner, E., Homam, S.M., Ackerman, L., Pfänder, J.A., Karimi, H., 2018. Geochemical and geochronological evidence for a Middle Permian oceanic plateau fragment in the Paleoe-Tethyan suture zone of NE Iran. *Contrib. Mineral. Petrol.* 173 (10) <https://doi.org/10.1007/s00410-018-1506-x>.
- Ustaömer, P.A., Ustaömer, T., Collins, A.S., Robertson, A.H.F., 2009. Cadomian (Ediacaran–Cambrian) arc magmatism in the Bitlis Massif, SE Turkey: Magmatism along the developing northern margin of Gondwana. *Tectonophysics* 473, 99–112.
- Valinasab Zarnagh, F., Moayyed, M., Jahangiri, A., Azizi, H., 2021. A gma source and the evolution of early Paleozoic (Silurian) metavolcanic rocks of Maku area (northwest of Iran): an evidence for Paleotethys drifting. *Petrology* 12 (45), 19–40.
- van Staal, C.R., and Barr, S.M. 2012. Lithospheric architecture and tectonic evolution of the Canadian Appalachians and associated Atlantic margin. Chapter 2. In *Tectonic Styles in Canada: The Lithoprobe Perspective*. Edited by J.A. Percival, F.A. Cook, and R.M. Clowes. Geological Association of Canada, Special Paper 49, pp. 41–95.
- Vesali, Y., Esmaeily, D., Moazzen, M., Chiaradia, M., Morishita, T., Soda, Y., Sheibi, M., 2020. The Paleozoic Jalal Abad mafic complex (Central Iran): implication for the petrogenesis. *Geochemistry* 80, 125597. <https://doi.org/10.1016/j.chemer.2020.125597>.
- Walter, M.J., 1998. Melting of garnet peridotite and the origin of komatiite and depleted lithosphere. *J. Petrol.* 39 (1), 29–60.
- Weaver, B.L., 1991. Trace element evidence for the origin of ocean-island basalts. *Geology* 19, 123–126.
- Wendt, J., Kaufmann, B., Belka, Z., Farsan, N., Karimi, B., Bavandpur, A., 2005. Devonian/Lower Carboniferous stratigraphy, facies patterns and palaeogeography of Iran. Part II: Northern and Central Iran. *Acta Geol. Pol.* 55, 31–97.
- Wilson, M., 1989. *Igneous Petrogenesis—A Global Tectonic Approach*. Unwin Hyman, London, p. 466p.
- Winchester, J.A., Floyd, P.A., 1976. Geochemical magma type discrimination; application to altered and metamorphosed basic igneous rocks. *Earth Planet. Sci. Lett.* 28, 459–469.
- Winchester, J.A., Floyd, P.A., 1977. Geochemical discrimination of different magmaseries and their differentiation products using immobile elements. *Chem. Geol.* 20, 325–342.
- Winchester, J.A., Pharaoh, T.C., Verniers, J., Ioane, D., Seghedi, A., 2006. Palaeozoic accretion of Gondwana-derived terranes to the East European Craton: recognition of detached terrane fragments dispersed after collision with promontories. *Geol. Soc. Lond.* 32, 323–333.
- Yang, H., Zhang, H.F., Luo, B.J., et al., 2015. Early Paleozoic intrusive rocks from the eastern Qilian orogen, NE Tibetan Plateau: petrogenesis and tectonic significance. *Lithos* 224–225, 13–31.
- Zhao, G., Wang, Y., Huang, B., Dong, Y., Li, S., Zhang, G., Yu, S., 2018. Geological reconstructions of the East Asian blocks: from the breakup of Rodinia to the assembly of Pangea. *Earth Sci. Rev.* 186, 262–286.
- Zindler, A., Hart, S., 1986. *Chemical Geodynamics*. Annual Review of Earth and Planetary Sciences 14, 493–571. <https://doi.org/10.1146/annurev.earth.14.050186.002425>.